2013

Controlling Factors on Bedrock River Sinuosity in the Eastern Tibetan Plateau

Lydia Curliss
Oberlin College

Controlling Factors on Bedrock River Sinuosity in the Eastern Tibetan Plateau

Lydia Curliss
Advisor: Amanda Schmidt
Oberlin College Spring 2013

Abstract

Average sinuosity of bedrock rivers across the eastern Tibetan Plateau (including the Yangtze, Mekong, Salween, Irrawaddy, and Tsang Po) ranges from 1.20-1.41. From 25°-30°N, sinuosity marginally increases east to west; over the entire distance of each river, sinuosity increases north to south. Increases in sinuosity parallel a regional tectonic gradient in an area with a marginal climate gradient. Several past studies correlate sinuous bedrock rivers in mountainous regions with gradients in climate, arguing that landslides are the main mechanism by which bedrock rivers increase sinuosity. Other studies find correlations between tectonics and increasing landslide frequency. To investigate the role of these and other factors in increasing bedrock river sinuosity, I tested correlations between river sinuosity and bedrock, landslides, climate, and erosion rates. I found no linear correlation between sinuosity and bedrock type, landslides, climate, or erosion rates. These results indicate that none of the proposed correlating factors are related to increasing sinuosity in this area, and that testing for other tectonic and geomorphic proxies including slope and mean local relief could provide insight.

Introduction

The study of landscape evolution focuses on investigating relationships between tectonics, climate, and erosion rates. This includes studying how tectonics and climate may force erosion rates. Some studies argue for tectonics or climate as the driving force on erosion, while other studies focus on the interrelationships between tectonics, climate, and erosion.

Numerous studies have found that tectonic forcing can drive erosion rates (Finnegan et al. 2008; Hetzel 2013; Larsen and Montgomery 2012; Montgomery and Brandon 2002). Finnegan et al. (2008) found a relationship between uplift and erosion rates, indicating that erosion rates increase to accommodate faster rates of uplift. Larsen and Montgomery (2012) looked at landslide erosion coupled to tectonics by mapping landslides and comparing them to exhumation rates, and found that landslide erosion rates are significantly coupled to exhumation and stream power— the potential of a river to incise into bedrock. Other studies have found relationships between areas of active faulting and erosion (Hetzel 2013) and that when relief has reached a maximum, continual uplift further increases erosion rates (Montgomery and Brandon 2002).

Similarly, climate has been found to affect erosion rates. Anders et al. (2008) found that precipitation patterns are a significant control of topography in the Himalaya. Montgomery et al. (2001) found a correlation between large-scale climate gradients and erosion rates in the Andes mountain range. Reiners et al. (2003) found that long-term erosion rates from apatite cooling ages in the Cascade Mountains follow annual precipitation rates. However, in tectonically active areas,

some studies have found that erosion rates are decoupled from climate gradients (Burbank et al. 2003).

One indicator of climate and tectonic influences on geomorphological processes are rivers. Rivers are categorized as alluvial or bedrock, and are an important geomorphological tool, removing material from an environment as more is brought in. Bedrock rivers in mountainous regions may be coupled to controls on landscape changes. For example, deeply incised bedrock rivers may be markers of large-scale landscape evolution (Hallet and Molnar 2001).

Alluvial rivers flow through sediments, which are generally soft and unconsolidated. Due to this, alluvial rivers are self-forming, and develop meanders over time, causing flow paths to become s-shaped. Sinuosity is used as way to quantify the amount that a river meanders. This measurement is a ratio of the actual river to the shortest distance between the end points (or the straight-line distances). The geometry of a meandering river consists of the cut-bank, point bar, and thalweg. The cut-bank is the outer curve of a meander where erosion or scouring of local rock/sediments occurs. The point bar is along the opposite side of the meander, and is the location of sediment deposition. The thalweg is the deepest part of the river where flow is the fastest. Over the span of a river, the thalweg shifts, creating scouring at the cut-bank.

In contrast to alluvial rivers, bedrock rivers cut directly through bedrock. This downward incision causes most bedrock rivers to have straight channel flow rather than sinuous flow patterns of alluvial rivers. Downward incision rather than the formation of meanders, classifies bedrock rivers as non-self-forming.

Figure 1: Map of study area, including (from east to west) the Yangtze, Mekong, Salween, Irrawaddy and Tsang Po rivers underlain by a DEM (Digital Elevation Model), which shows elevations across the area. The inset shows the location of the five rivers within the Asian continent.

Studies show that the rate of down-cutting is affected by the amount of sediment cover in the bed. Sklar and Dietrich (2001) have shown that larger sediment grain sizes (>35mm) result in reductions in erosion, and that large influx of sediment can cause down-cutting to cease.

In some circumstances, bedrock rivers are sinuous because sinuosity is antecedent to uplift. During uplift, a meandering river may be elevated, such as rivers in the four corners region of the United States. Due to the river's higher elevation, erosion increases in order for the river to reach base level, causing the river to maintain its former flow path.

In other cases, bedrock rivers may have sinuosity that postdates uplift. In these situations, rivers start with a straight flow path, but become sinuous due to outside factors that cause erosion of the bedrock via undercutting. Undercutting is most common on the outside of small bends in the river because that is where the thalweg is closest to the river bank. This leads to slope failure and mass wasting events, thus increasing river sinuosity.

Stark et al. (2010) proposed that bedrock strength and a climate gradient (storminess) best correlate with bedrock river sinuosity in Taiwan, Japan, and the Philippines. Storminess is based upon the number of storms or typhoons that occurred across these areas on 20-30 year timescales. Their study used Digital Elevation Models (DEMs) to extract stream networks in order to measure sinuosity. They found a correlation between bedrock strength, sinuosity and storminess. They also argued that if tectonics played a role in changing sinuosity, it should vary across Japan, but found that there was no correlation to the tectonic gradient.

In a single study area, to test possible factors correlating to sinuosity, including tectonics, I chose to look at rivers in the eastern Tibetan Plateau. This area contains five large, sinuous rivers. From east to west, these rivers are the Yangtze, Mekong, Salween, Irrawaddy, and Tsang Po (Figure 1). This area is an ideal study area because it has a strong tectonic gradient and weak climate gradient from 25°N-30°N. The tectonic gradient here is inferred from previous studies of exhumation and erosion rates in the area (Henck et al. 2011). I determined correlations between sinuosity and bedrock, landslides, rainfall, and erosion rates.

Study Area

The eastern Tibetan Plateau is located at the edge of the collision between the Indian and Eurasian plates. The collision began at ~55-50 Ma, but its current movement regime is thought to have begun at ~15-10 Ma (Royden et al. 2008). The area is shortening north to south and extending east to west. Studies of the collision between the Indian and Eurasian plates have produced several hypotheses for plate motion. In general, two end member hypotheses exist to explain movement of Tibet— the crustal block hypothesis and crustal flow hypothesis.

The crustal block hypothesis proposes that a series of fault systems in eastern Tibet accommodate plate movement. It is observed that there are a series of typical strike-slip faults in eastern Tibet that are indicators of the east-west extension (Figure 2a). Tapponier et al. (2001) proposed these fault systems are accommodating the eastward movement of the plateau.

Figure 2a: From Tapponier et al. (2001), this map shows major fault zones that are proposed to be accommodating eastward extension of the Tibetan Plateau.

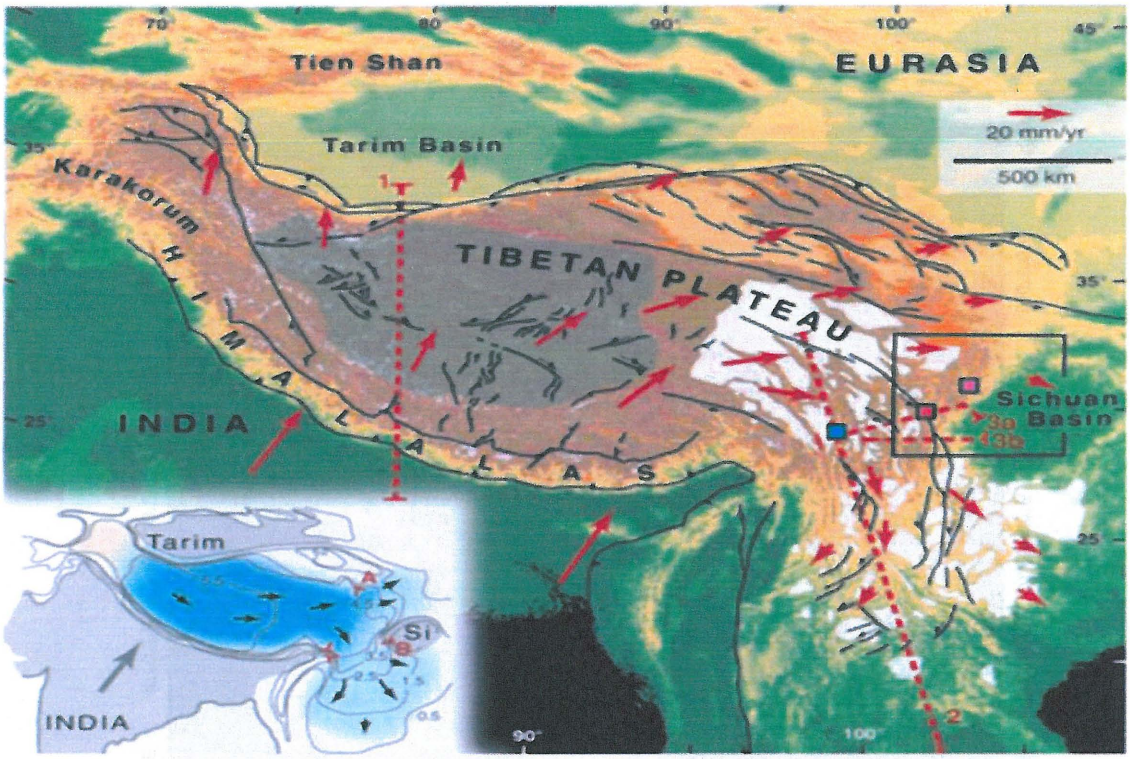

Figure 2b: From Royden et al. (2008) this map shows the relative movement of the Tibetan plateau. The inset demonstrates the movement direction proposed by crustal flow model.

The crustal flow hypothesis is based on a partially molten lower crust accommodating east to west extension (Royden et al. 2008). In order for the lower crust to flow, material must be warm and relatively weak. Royden et al. (2008) hypothesizes that in this case, the lower crust is flowing toward the eastern margin of the Tibetan Plateau due to extension of the crust (Figure 2b).

A modified version of the crustal flow hypothesis is the channel flow hypothesis. Like crustal flow, channel flow assumes the lower crust is partially molten, relatively weak, and moving eastward (Hodges 2006). For this hypothesis, Hodges (2006) proposes that eastward movement is accommodated by channelized flow through weak parts of the crust.

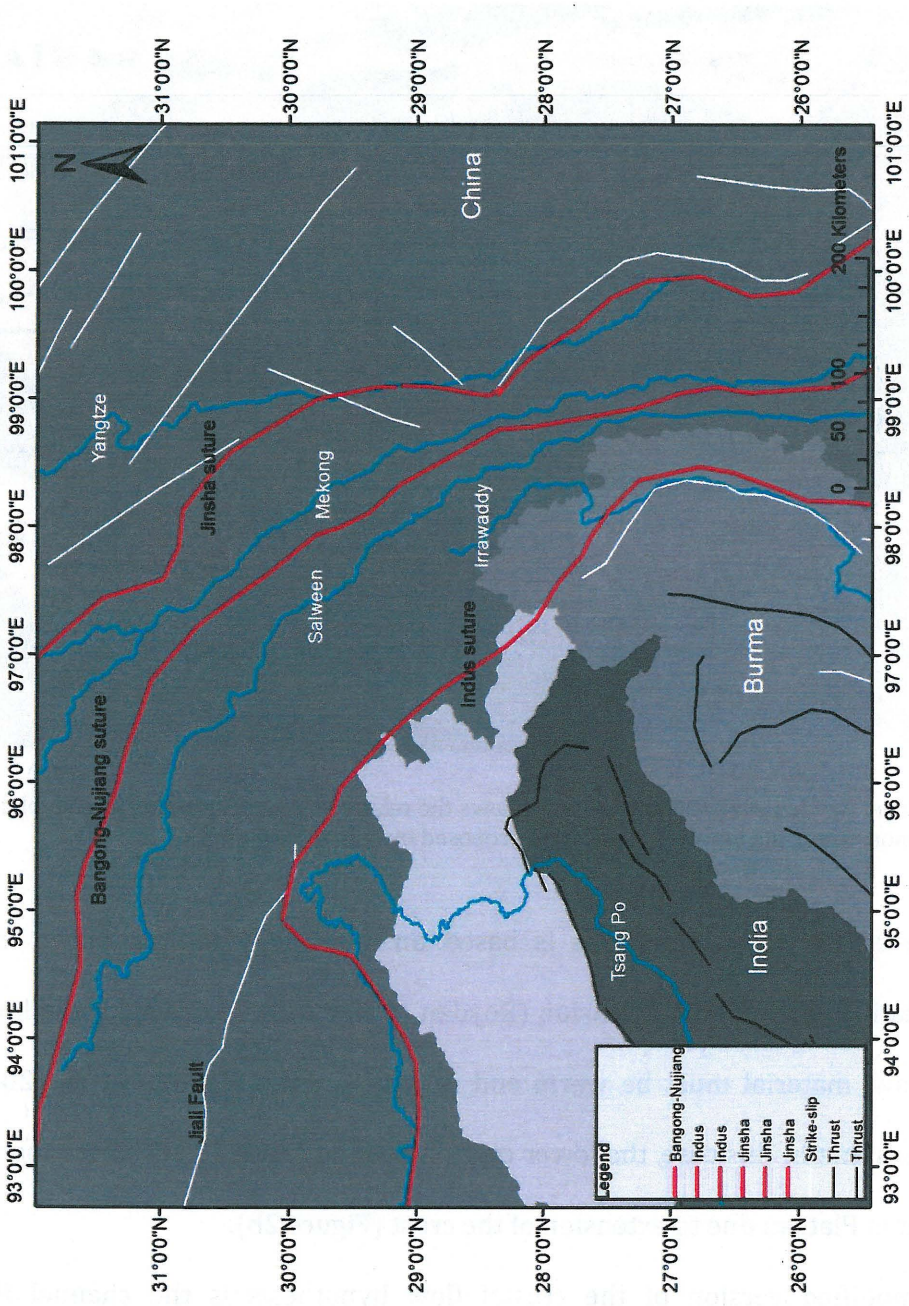

Figure 3: Simplified version of tectonic features mapped by Taylor and Yin (2009). This map includes thrust faults, strike-slip faults and major suture zones within the study area.

Various studies have investigated movement of the Tibetan Plateau. Zhang et al. (2004) found that material within the plateau is moving roughly eastward before it is diverted south around the eastern edge of the Himalayan range. Shen et al.

(2005) used GPS data to determine that eastern Tibet has a series of microblocks that rotate in a way that indicates a mechanically weak crust rather than movement by faulting.

Several suture zones, as well as zones of compression, strike-slip and thrust faulting, define the eastern Tibetan Plateau. Geology here reflects eastward movement of the plateau caused by N-S shortening, and has been mapped by Taylor and Yin (2009) (Figure 3).

Strike-slip faults and thrust faults exist throughout the study area. To the east of the Yangtze are two faults that border the Sichuan basin: the Longmen Shan, a thrust fault with a south trending trace; and the Xianshuihe, a strike-slip fault with a southeast trending trace. To the south of the Yangtze, Mekong, and Salween rivers is the Red River fault, a strike-slip fault with a southeast trending trace. To the north of these rivers is the Kunlun fault, a strike-slip fault at the southern margin of the Qaidam Basin with an east trending trace. To the north of the Tsang Po is the Jilali fault, a strike slip that has a southeast trending trace (Hetzel 2013; Tapponier 2001).

Suture zones are boundaries between distinct tectono-stratigraphic terranes (foreign material) that are accreted onto continents during collisional events (Bierman and Montgomery 2013). In the eastern Tibetan Plateau, a series of suture zones exist, where accreted terranes are increasingly younger east to west. The Jinsha suture zone formed during the Triassic (Yang et al. 2012), and trends roughly north to south, cutting across the Yangtze River. Between the Mekong and Salween is the Bangong-Nujiang suture formed during the Mesozoic, it was reactivated

during the Cenozoic (Harrison and Yin 2000). Movement of faults surrounding this suture zone is proposed to accommodate east to west extension of the Plateau (Taylor et al. 2003). Between the Irrawaddy and Tsang Po is the Indus suture that trends east to west, cutting across the Irrawaddy where it trends north to south. The Indus suture was believed to have been formed after ~46 Ma (Harrison and Yin 2000).

From east to west, the blocks in this area include the Kunlun block, Qiangtang block, Lhasa block, and Himalayan block (Gan et al. 2007). The bedrock is composed of several units that include intrusive igneous rocks, metamorphosed rocks, and sedimentary rocks. The bedrock underlying the Yangtze, Mekong, and Salween rivers includes carbonates, sandstones, schists, quartzites, monzonitic granites, limestone, diabase, and clastics, ranging in age from Precambrian to Cenozoic (Ackiz et al. 2008; Map Compilation Group 1986).

A number of studies have found that exhumation rates are useful proxies for uplift (Booth et al 2009; Burg et al. 1997; Ding et al. 2001; Clark et al. 2005). Exhumation is measured using thermochronometry dating to determine the time it has taken a rock unit to reach the surface. These ages are used in combination with thermal models of the crust to infer uplift on $10^5 \geq$ year time scales. Henck et al. (2011) compiled exhumation rates from past studies for eastern Tibet. This compilation shows that exhumation rates mimic regional patterns in tectonic activity, correlating exhumation to rates of uplift. Rates are higher in the west (10 mm/yr over the last 10 ma) and decrease to the east (0.25-0.65 mm/yr from about 9-13 ma) (Figure 4).

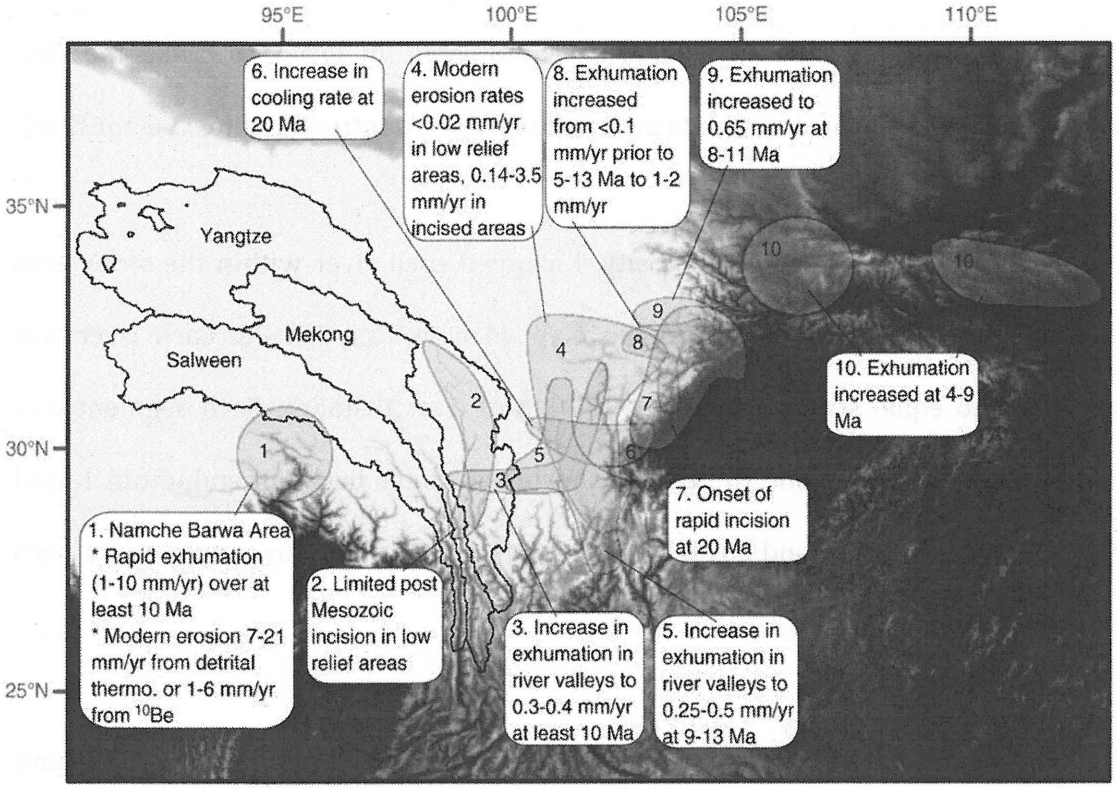

Figure 4: From Henck et al. (2011), map showing collective exhumation rates determined from previous studies.

Methods

The main methods in this study were designed to quantify sinuosity and possible controlling parameters. Many of my analyses were done in ESRI's ArcGIS 10, a geographical information systems program, that allows for the integration and analysis of spatial datasets. I used Google Earth and ArcGIS to map chosen parameters in the study area from 25°-30°N. Rivers and landslides were mapped in Google Earth and imported into ArcGIS, where bedrock, rainfall, and erosion rates were added to investigate potential correlations.

All data that I used were georeferenced in order to analyze them together in the same geographic locations. Georefrencing is the process of establishing an image in physical space based on geographic coordinates. In order to make the data compatible with GIS analyses, data sets were converted into shapefiles (vector files).

Sinuosity

In order to determine sinuosity, I mapped each river within the study area using Google Earth and imported the mapped lines into ArcGIS. Each river was divided into equal study reaches of ~50 km of river distance. Each segment was measured from end to end to find the shortest distance between endpoints. I used the actual river length and straight-line length to determine the sinuosity for each study reach.

Indicators of Sinuosity

Past studies (Mumipour et al. 2012; Stark 2006; Stark et al. 2010) have suggested that different factors, such as climate and tectonics, influence sinuosity in bedrock rivers. For this study, I explored how bedrock, rainfall, landslide frequency and erosion rates correlate with sinuosity. Correlations between these factors may indicate the relative importance of each parameter in increasing sinuosity.

Table 1: Bedrock categories and associated key.

Rock Category	Key
Carbonate	1
Pelitic	2
Feldspar Granite	3
Sedimentary	4
Mafic	5
Unmerged/Unclassified	6

Bedrock

Bedrock strength controls incision rates (Hartshorn et al. 2002; Sklar and Dietrich 2001). Bedrock strength is an important possible factor because its variation could cause discrepancies in lateral incision rates, which could in turn affect the rates at which meanders form.

I simplified bedrock maps of the Three Rivers Region (Map Compilation Group 1986) and the Tsang Po (Booth at al. 2009) by grouping together 43 mapped units into groups of similar lithology and mineralogy. Each unit that intersected one or more of the rivers was approximated with individual polygons, drawn using the boundaries from the rock units on the bedrock map, and categorized into one of six rock groups. The categories used were carbonates, pelitic (sheet silicate rich rock), granite, sedimentary, mafic, and unmerged/unclassified (Table 1, 2). These groups were determined by the primary rock type listed for each unit. Though they may not correspond exactly to the rock indicated by the group designation, it is thought that they will erode similarly. For example, marble is classified as a carbonate even though it is also metamorphic.

The mapped bedrock polygons and rivers were intersected in ArcGIS. The intersect tool was used to determine sinuosity for each bedrock unit, by looking at where the river overlapped individual units. In order to correlate bedrock to sinuosity, I looked at all sinuosity measurements for each bedrock type in all the rivers. In order to quantify these relationships, I created box plots in Microsoft Excel 2011 in order to show the distributions of sinuosity across each of the aforementioned bedrock types.

Table 2. All mapped rock units by description copied directly from the bedrock map. Note "-----" indicates no information available.

Symbol	Description	Key
D2+3	Carbonate rocks (w/ volcanics and shale)	1
D2-3	Carbonate rocks (w/ volcanics and shale)	1
D1	Carbonate rocks and sandstone	1
€2-3	Slates with carbonates	2
P1	Carbonate rocks, limestone	1
AnD	Schists, quartzites, and marble	2
Q	Alluvial, lacustine, slope wash, glacial deposits	6
C2+3	Limestone; sandstone and slate	1
P2	Carbonate, clastic, siliceous	1
P2/1	Intermediate-basic volcanic rock	5
P1/1	Basalt, siliceous, mica-quartzite?, schist and marble	5
D	Undivided or merged	6
P2b/1	Metamorphic, intermediate-basic volcanic rocks	5
P2O/1	Limestone, clastic rocks	1
Yo3/4	Plagiogranite, granodiorite	3
S	Carbonate or metamorphic casolites	1
Yδ4	Granite, granodiorite	3
T1	Limestone, sandstone and slate	1
C	Undivided or merged	6
T2b/3	Slates, sandstone and intermediate-acidic volcanic rocks	2
Pz2	Metamorphic intermediate-basic volcanic-sedimentary rocks	5
Yn3/5	Monzontitic granite, granodiorite	3
Yx3/5	Granite, K-feldspar granite	3
K1/1	Mudstone, siltstone, sandstone	4
K2/1	Sandstone, siltstone	4
J2	Mottled mudstone, siltstone, marl, limestone	4
J3	Purple/red clastic rocks	4
K1	Purple/red sandstone, siltstone	4
T2/2-T1/3	Sandstone, slate, pebble sandstone	4
v2/5	Gabbro, undivided basic rock	5
Yπ1/6	Granitic porphyry, subrhyolitic porphyry	3
v1/5	Gabbro, diabase	5
J1-O/2	Sandstone, shale	4
C1	Limestone	1
T2	Clastic rocks with limestone; carbonate and clastic	4
C3	Carbonate rocks or clastic	1
Ptgl	Migmatites, gneisses, leptynites, marble and quartzite	3
Yn2-3/5	K-feldspar granite, monzonitic granite	3
J2-3	Grey-black clastic with limestone	4
Pz	Lower grade metamorphic clasolites, schists, phyllites, marble	2
Tethyan-Himalyan	metasediments	4
Gangdese plutons	granodiorite	3
-----	Migmatites and mylonitic gneisses	3

Landslides

Landslides are a proposed mechanism by which landscapes change, and landslide frequency and size has been found to correlate with tectonics and climate (Larsen and Montgomery 2012; Stark et al. 2010). Undercutting of the cut-bank is proposed to cause slope failure due to loss in stability, thus increasing sinuosity through lateral erosion. Formation of sediment via landsliding enables continual undercutting and lateral erosion to take place by causing slope material to become unconsolidated and weak. Correlating landslides to sinuosity could indicate a relationship to tectonics and/or climate and determine whether it is a mechanism for which rivers become more sinuous.

To measure landslide frequency, I mapped landslides along the rivers in Google Earth. In order to determine what features were landslides, I looked for slopes along the rivers that were barren and had large deposits of sediments along the riverbanks. In some cases these were easily identifiable, but some were guesses based on differences from the surrounding image. Landslide area and river sinuosity were compared to look for a potential correlation between higher rates of sinuosity and higher landslide frequency. In order to do this, each landslide area was measured in ArcGIS, and a total landslide area was found for each study reach. For each segment, total landslide area was plotted against sinuosity to determine r^2 and p-values for each river and for the entire study area.

Climate

Climate is often proposed as a control on the evolution of landscapes. Stark et al. (2010) found a positive correlation between rainfall and river sinuosity in Taiwan and Japan, using storminess (the number of typhoons) as a climate

indicator. Often modern mean annual rainfall is used as a measure of climate, and is correlated to erosion rates in some places (Anders et al. 2006; Anders et al. 2008; Montgomery et al. 2001; Reiners et al. 2003). I quantified climate using mean annual rainfall data for the years 2000-2006 from the Tropical Rainfall Measuring Mission (TRMM) satellite. TRMM data is stored in 1x1 km pixels, where each pixel has an average rainfall quantity. These data were processed using methods described by Anders et al. (2006). I used rainfall as a proxy for the monsoon climate that exists across the area. A monsoonal climate indicates that there is effectively 1 storm per year. In order to look at how rainfall and river sinuosity is correlated, TRMM data was compared to sinuosity over study reaches. In order to correlate rainfall to sinuosity, averages from the TRMM data were plotted against sinuosity per each river section. For each river and for the entire study area, r^2 and p-values were determined.

Erosion Rates

Erosion rates may be related to sinuosity because of possible correlations between erosion rates and landslides, climate, and tectonics. Furthermore, broad patterns in erosion rates are found to mimic the tectonic gradient in the study area (Henck et al. 2011). Therefore, if increased tectonic activity is correlated with sinuosity, higher erosion rates should correlate to higher sinuosities. Data from erosion come from Henck et al. (2011), and are not available for the Irrawaddy or Tsang Po.

In situ ^{10}Be forms in quartz crystals at a fixed rate per year when they are within 2 meters of the surface. The concentration of ^{10}Be in river sand collected

downstream represents a spatial average of the erosion rate in the upstream watershed (Brown et al. 1995; Bierman and Steig 1996; Granger et al. 1996). *In situ* ^{10}Be-derived erosion rates follow similar trends across the Yangtze, Mekong and Salween. For each drainage basin, erosion rates generally increase north to south and across the whole area, increase east to west (Henck et al. 2011)

In order to correlate erosion rates with sinuosity, I used ArcGIS to intersect the Yangtze, Mekong and Salween with the erosion rate for each study reach, and determined sinuosity for each intersected section. Sinuosity and erosion were plotted and r^2 and p-values were determined for the Yangtze, Mekong and Salween rivers.

Results

Results for sinuosity and its parameters, including bedrock type, landslides, climate, and erosion rates are summarized in Table 3. Average sinuosity over the area ranges from 1.20-1.41, following an increasing east to west trend. Over the entire study area and most individual rivers, sinuosity is not linearly correlated to any tested parameter.

Table 3: Summary of sinuosity, bedrock, landslide, climate and erosion rate data collected for this study.

	Sinuosity	Bedrock	Landslides	Climate	Erosion Rate
Yangtze	Average sinuosity is 1.20 with a range from 1.13-1.34 and a standard deviation of 0.06.	Five bedrock types are prevalent: carbonates, pelitic, granites, mafic and unmerged/unclassified.	54 total landslides, total area is $1.53x10^9$ m^2; average per landslide is $2.85x10^7$ m^2 with a standard deviation of $1.97x10^5$ m^2.	Rainfall ranges from 518-866 mm/yr with a mean of 607 mm/yr and a standard deviation of 96 mm/yr.	Erosion rates range from 0.04-0.043 mm/yr.
Mekong	Average sinuosity is 1.26 with a range from 1.08-1.52 with a standard deviation of 0.04.	Four bedrock types are prevalent: carbonates, sedimentary, mafic and unmerged/unclassified.	56 total landslides, total area is $1.21x10^9$ m^2; average area per landslide is $2.15x10^7$ m^2 with a standard deviation of $1.27x10^5$ m^2.	Rainfall ranges from 473-1020 mm/yr with a mean of 743 mm/yr and a standard deviation of 206 m/yr.	Erosion rates range from 0.2-0.5 m/yr.
Salween	Average sinuosity is 1.31 with a range from 1.09-1.91 and a standard deviation of 0.17.	Five bedrock types are prevalent; carbonates, pelitic, granites, sedimentary and unmerged/ unclassified.	41 total landslides, total area is $1.60x10^9$ m^2; average area per landslide is $3.91x10^7$ m^2 with a standard deviation of $1.82x10^5$ m^2.	Rainfall ranges from 512-1142 mm/yr with a mean of 881 mm/yr and a standard deviation of 237 mm/yr.	Erosion rates range from 0.8-8.0 mm/yr.
Irrawaddy	Average sinuosity is 1.40 with a range from 1.06-2.61 and a standard deviation of 0.40.	Two bedrock types are prevalent: carbonates and granites.	18 total landslides, total area is $1.28x10^8$ m^2; average landslide per area is $7.084x10^6$ m^2 with a standard deviation of $1.89x10^4$ m^2.	Rainfall ranges from 693-1634 mm/yr with a mean of 1306 mm/yr and a standard deviation of 305 mm/yr.	No data
Tsang Po	Average sinuosity is 1.41 with a range from 1.15-2.06 and a standard deviation of 0.24.	Three bedrock types are prevalent: granite, sedimentary and mafic.	40 total landslides, total area is $6.39x10^8$ m^2; average landslide per area is $1.60x10^6$ m^2 with a standard deviation of $5.06x10^4$ m^2.	Rainfall ranges from 568-2355 mm/yr with a mean of 1535 mm/yr and a standard deviation of 560 mm/yr.	From 29 19'14.39 to 29 19'35.03 the erosion rate is 1.71 mm/yr.

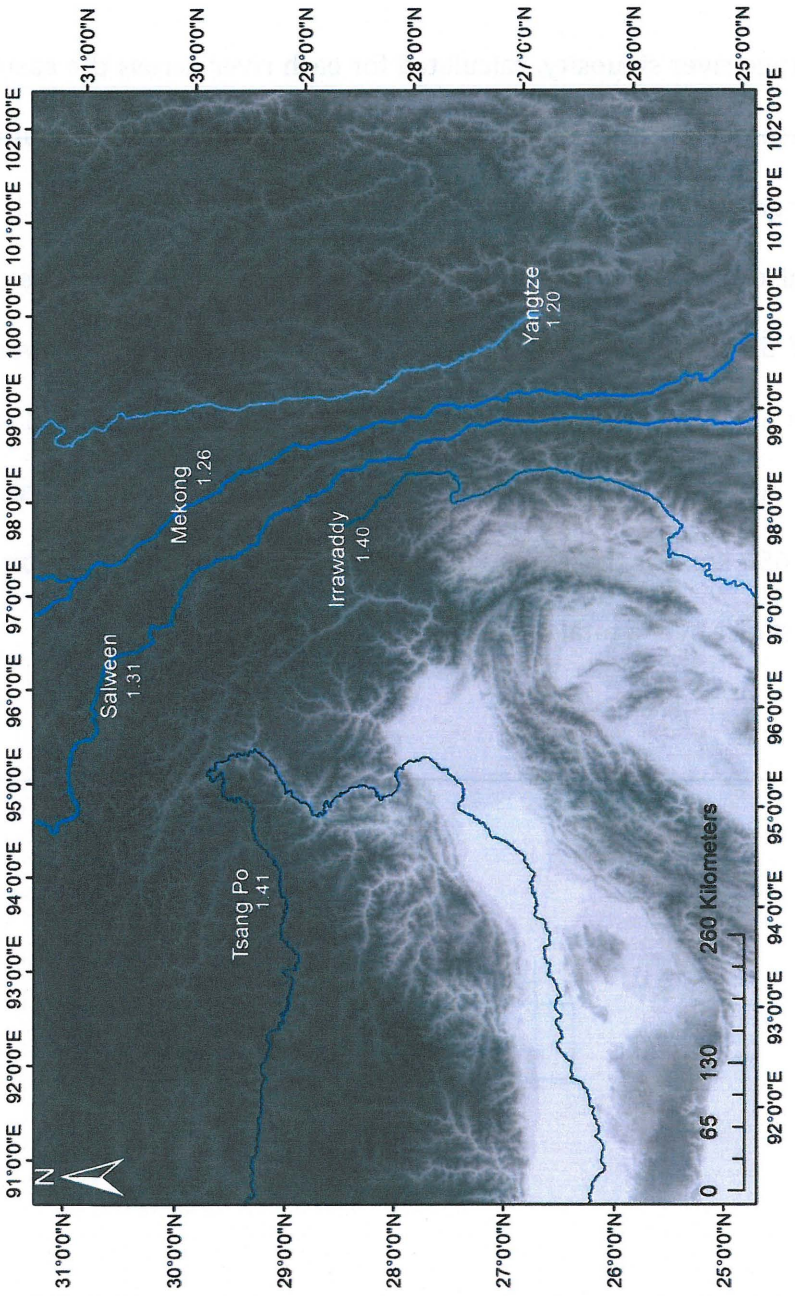

Figure 5: Rivers across the study area by sinuosity. Sinuosity increases east to west (from the Yangtze to the Tsang Po) from 1.20-1.41.

Sinuosity

Average river sinuosity, calculated for each river across the eastern Tibetan Plateau ranges from 1.20-1.41, increasing east to west and north to south (Figure 5). For the Yangtze, average river sinuosity is 1.20 for 11 sections of 50 km distances over a total of 547 km. For the Mekong, average river sinuosity is 1.26 for 18 sections of 52 km over a total distance of 936 km. For the Salween, average sinuosity is 1.31 for 19 sections of 48 km, for a total distance 912 km. For the Irrawaddy, average river sinuosity is 1.40 for 13 sections over 50 km for a total distance of 650 km. For the Tsang Po, average river sinuosity is 1.41 for 33 sections of 53 km distance over a total of 1749 km (Figure 6).

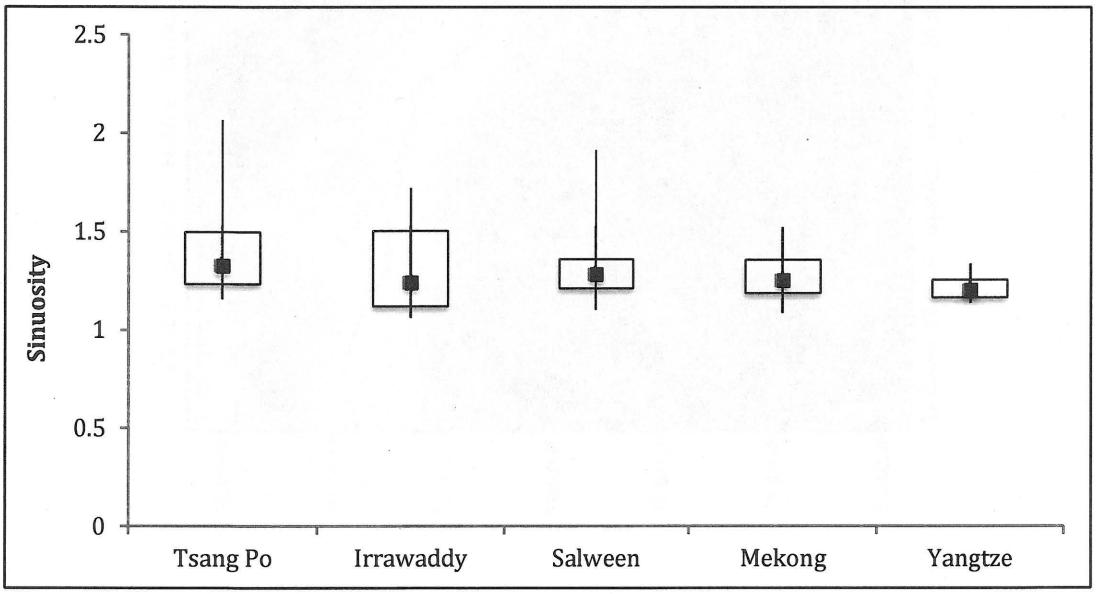

Figure 6: Box and whisker plot showing all sinuosity measurements for each river. Boxes in this graph highlight the middle portion of the data. The square represents the median, and the whiskers indicate the range between the minimum and maximum values.

Table 4: Summary of all bedrock units in each category for each river.

	Carbonate (1)	Sheet Silicates (2)	Feldspar Granite (3)	Sedimentary (4)	Mafic (5)	Unmerged/ Unclassified (6)
Yangtze	D2+3, P1, C2+3, P2, P2O/1, D2-3	e2-3, AnD	Yo3/4, Yδ4	N/A	P1/1, P2/1, P2b/1	D
Mekong	P1, C1	N/A	N/A	J2, K1/1, J3, K2/1, K1, T2/2-T1/3, J1-O/2	v2/5	Ptch, Yn1/6, D, C, Yn2/5
Salween	C1, C3, P1	Pz	Ptgl, Yn2-3/5	T2, J2, J3, K1, J2-3	N/A	C
Irrawaddy	C2+3	N/A	Yn3/5, Yx3/5	N/A	N/A	N/A
Tsang Po	N/A	N/A	Gneisses, Pluton, Migmatite gneisses	TH-metaseds	Suture	N/A

Bedrock

All bedrock units have been classified as carbonates, pelitic, granites, sedimentary, mafic, or unmerged/unclassified. Units that have been classified can be found compiled in Table 2, and are based upon data from the two maps of the area (Booth et al. 2009; Map Compilation group 1986) .

The Yangtze cuts through 14 types of bedrock, including six carbonate units, two pelitic units, two granite units, three mafic units and one unmerged/ unclassified unit. The Mekong cuts through 15 types of bedrock, including two

carbonate units, seven sedimentary units, one mafic unit, and five unmerged/unclassified units. The Salween cuts through 12 types of bedrock, including three carbonate units, one pelitic unit, two granite units, five sedimentary units, and one unmerged/unclassified unit. The Irrawaddy cuts through three types of bedrock, including one carbonate unit, and two granite units. The Tsang Po cuts through five types of bedrock, including three granite units, one sedimentary unit, and one mafic unit (Table 4; Figure 7).

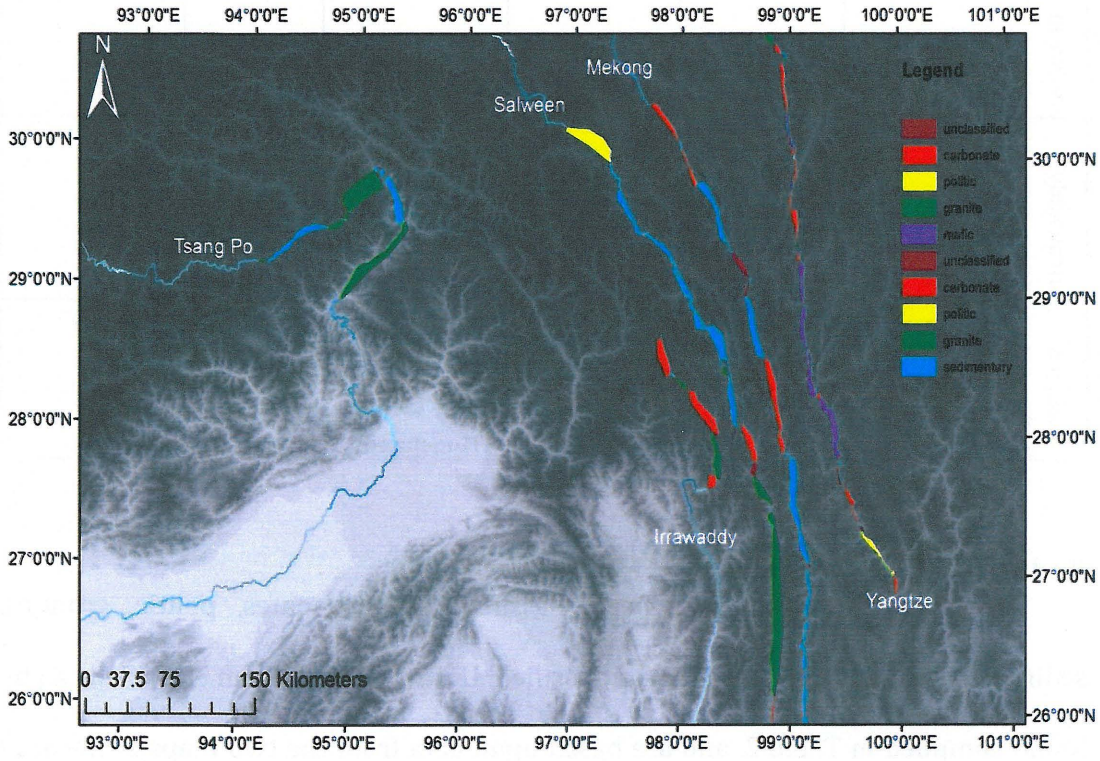

Figure 7: Map showing distributions of different bedrock types across the study area. Each color is a different category where orange are carbonate, yellow are pelitic, green are granite, blue are sedimentary, purple are mafic, and red are unclassified.

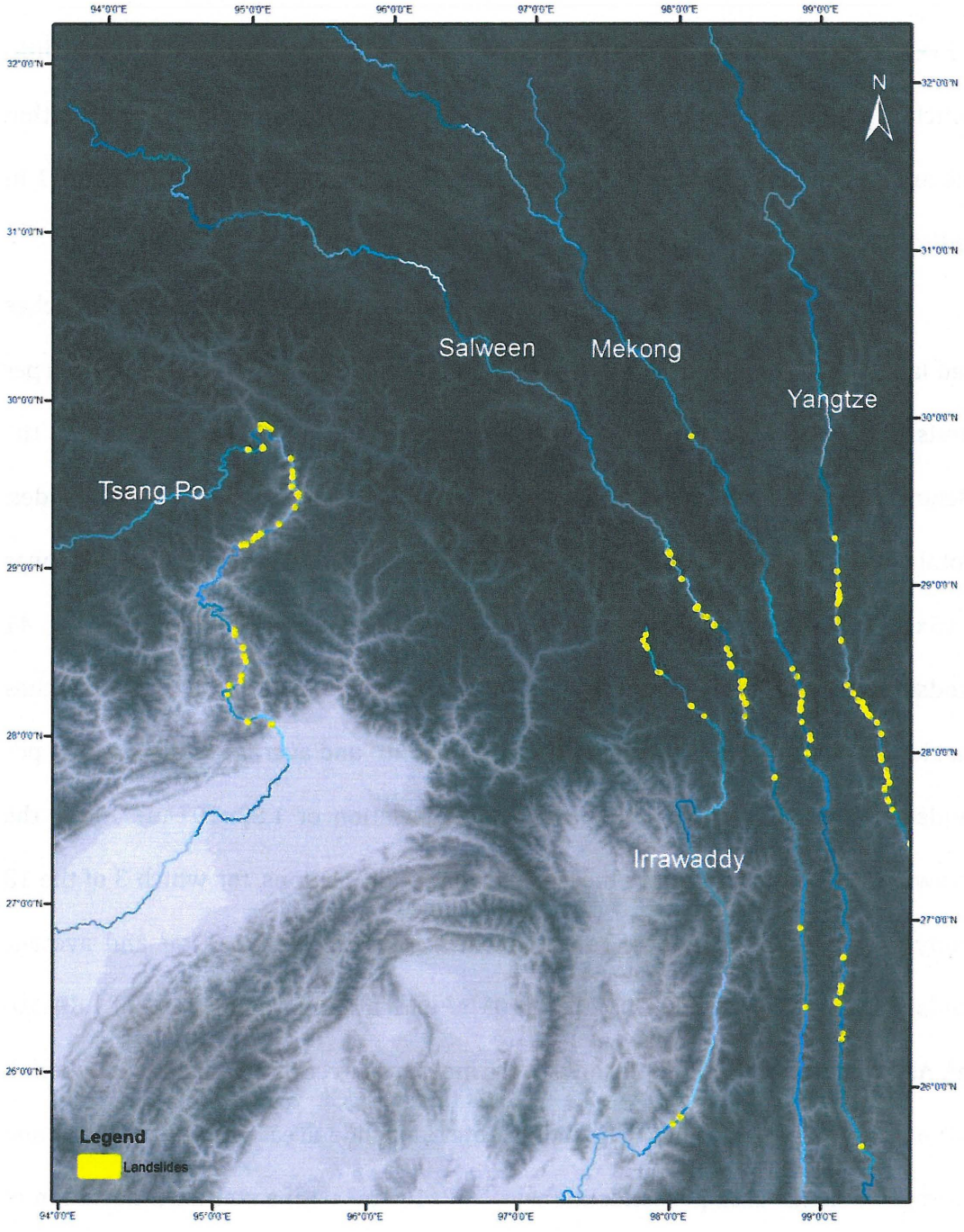

Figure 8: Landslides mapped across the area in yellow, their areas have been exaggerated (10x) to show dispersal across the rivers.

Landslides

Over the study area, 209 landslides were measured with a total area of 5.11×10^9 m^2 (Figure 8). Landslides occur in every bedrock type except in pelitic, which is probably due to the fact that it is the least common rock category within the area. Of these landslides, 49 occur in carbonate units, 21 in granite units, 51 in sedimentary units, 38 in mafic units, and 1 in an unmerged unit.

Along the Yangtze, 54 landslides were measured; 6 out of 11 study reaches had landslides. Total landslide area was 1.53×10^9 m^2 and average landslide area per landslide was 2.85×10^7 m^2 with a standard deviation of 1.97×10^5 m^2. Along the Mekong, 56 landslides were measured; 6 out of 18 study reaches had landslides. Total landslide area was 1.21×10^9 m^2 and average landslide area per landslide was 2.15×10^7 m^2 with a standard deviation of 1.27×10^5 m^2. Along the Salween, 41 landslides were measured over 48 km distances, where 7 out of 19 study reaches had landslides. Total landslide area was 1.60×10^9 m^2 and average landslide area per landslide was 3.91×10^7 m^2 with a standard deviation of 1.82×10^5 m^2. Along the Irrawaddy, 18 landslides were measured over 50 km sections, for which 3 of the 13 study reaches had landslides. Total landslide area was 1.28×10^8 m^2 and average landslide area per landslide was 7.084×10^6 m^2 with a standard deviation of 1.89×10^4 m^2. Along the Tsang Po, 40 landslides were measured over 53 km distances, where 8 out of 34 study reaches had landslides. Total landslide area was 6.39×10^8 m^2 and average landslide area per landslide was 1.60×10^6 m^2 with a standard deviation of 5.06×10^4 m^2.

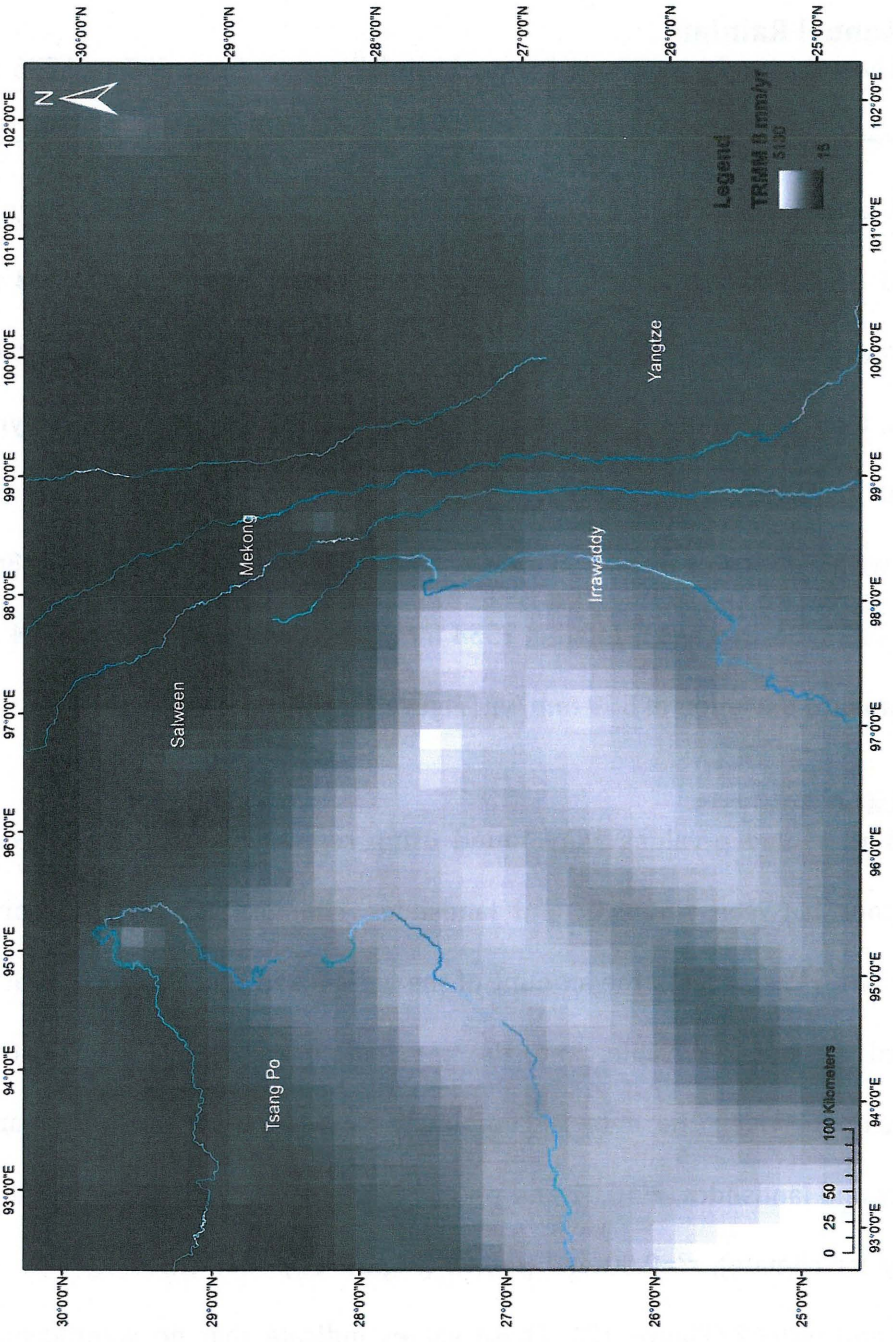

Figure 9: Map of rivers by ~50 km sections with TRMM data. Each pixel represents a 1x1 km area, and average rainfall ranges from 15 mm/yr to 5130 mm/yr.

Mean Annual Rainfall

Over the study area, mean annual rainfall ranges from 607 to 1535 mm/yr with an average of 1120 mm/yr and a standard deviation of 528 mm/yr. For the Yangtze, average rainfall is 6.07 mm/yr with a range of 518-866 mm/yr and a standard deviation of 81 mm/yr. For the Mekong, average rainfall is 743 mm/yr with a range of 473-1020 mm/yr and a standard deviation of 206 mm/yr. For the Salween, average rainfall is 881 mm/yr with a range of 512-1142 mm/yr and a standard deviation of 237 mm/yr. For the Irrawaddy, average rainfall is 1306 mm/yr with a range of 693-1633 mm/yr and a standard deviation of 318mm/yr. For the Tsang Po, average rainfall is 1534 mm/yr with a range of 576-2354 mm/yr and a standard deviation of 559 mm/yr (Figure 9).

Regression Analysis

Both r^2 and p-values were found using regression analyses to determine correlations between sinuosity and landslides, climate, and erosion. For linear correlations, r^2 represents the amount of the variance in the y-variable that can be explained by the x-variable, and the p-value shows the likelihood that the relationship between the data is completely random. Over the whole area, for sinuosity and landslides, $r^2=0.01$ and $p=0.55$ (Figure 10). For sinuosity and rainfall (a proxy for climate), $r^2=0.00$ and $p=0.68$ (Figure 11). For sinuosity and erosion, $r^2=0.01$ and $p=0.62$ (Figure 12). These values indicate that no significant, linear correlations exist between sinuosity and the studied parameters (mean annual rainfall, landslides, and erosion); sinuosity values also are not statistically different across different bedrock units.

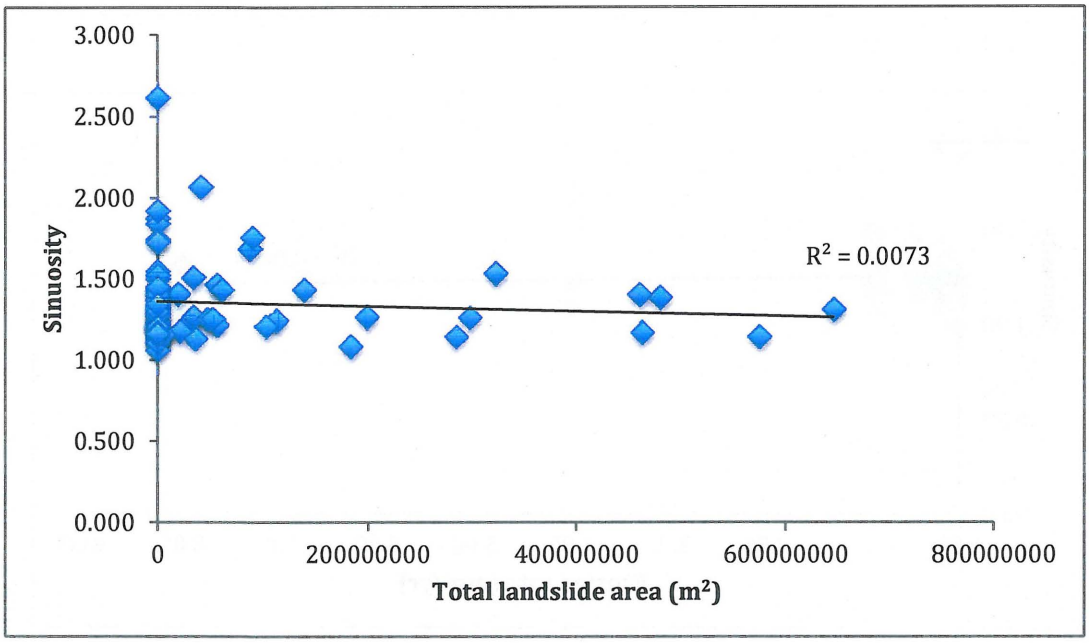

Figure 10: Graph of the linear correlation between landslide area and sinuosity. No linear correlation exists, and r^2=0.01 and p=0.55.

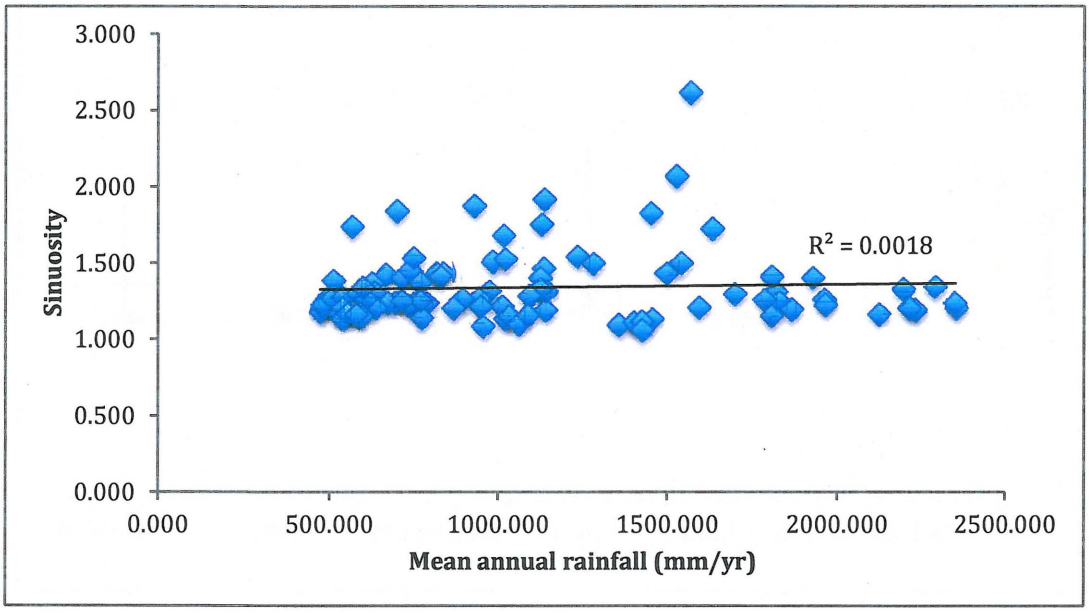

Figure 11: Graph of linear correlation between mean annual rainfall and sinuosity. No linear correlation exists, and r^2=0.00 and p=0.68.

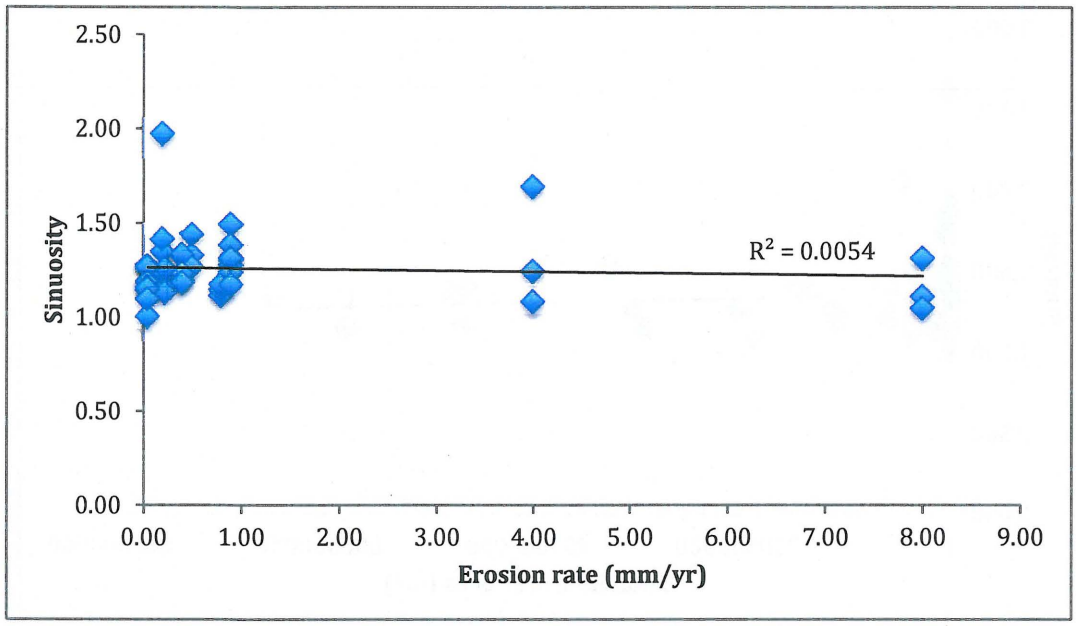

Figure 12: Graph of linear correlation between erosion rate and sinuosity for the Yangtze, Mekong and Salween. No linear correlation exists, and r^2=0.01 and p=0.62.

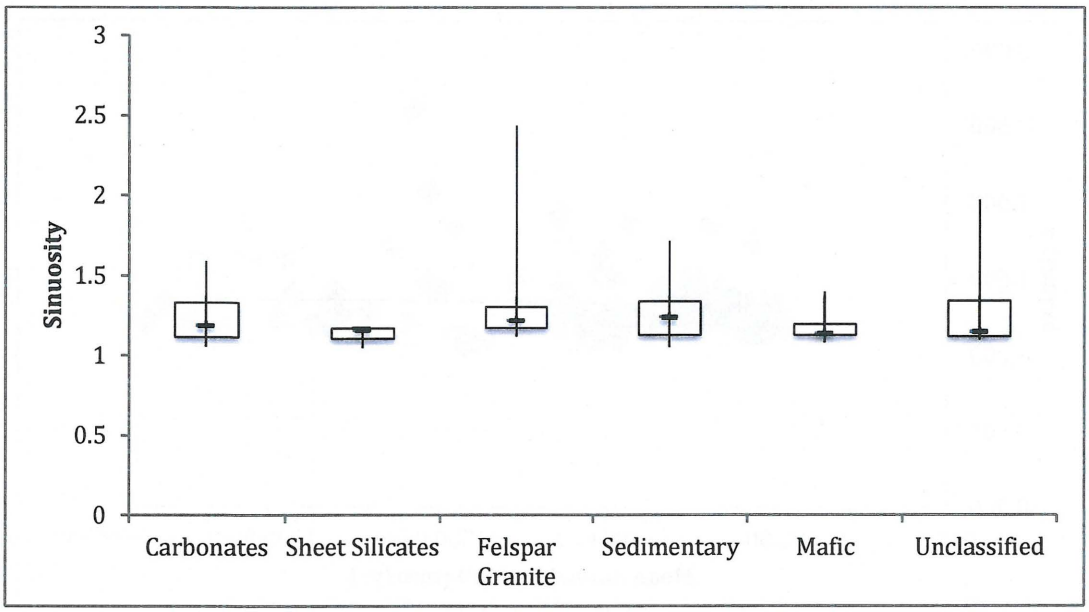

Figure 13: Box and whisker plot showing all sinuosity measurements for each bedrock type including data from all rivers. Boxes in this graph highlight the middle portion of the data. The square represents the median, and the whiskers indicate the range between the minimum and maximum values.

There is not a correlation between bedrock type and sinuosity. A box plot was made to show all of the sinuosity per each bedrock type (Figure 13). Median values for bedrock, given by bedrock type, are as follows: 1.19 for carbonates, 1.16 for pelitics, 1.22 for granites, 1.23 for sedimentary, 1.14 for mafic and 1.14 for unmerged/unclassified.

For landslide area and sinuosity (Appendix A), the Yangtze has an r^2=0.09 and p=0.36. For the Mekong, the r^2=0.00 and p=0.87. For the Salween, the r^2=0.02 and p=0.56. For the Irrawaddy, the r^2=0.02 and p=0.67. For the Tsang Po, the r^2=0.12 and p=0.05. With the exception of a weak correlation in the Tsang Po River, landslide area and sinuosity are not linearly correlated.

For rainfall and sinuosity (Appendix B), the Yangtze has an r^2=0.09 and p=0.37. For the Mekong, the r^2=0.02 and p=0.58. For the Salween, the r^2=0.00 and p=0.85. For the Irrawaddy, the r^2=0.03 and p=0.82. For the Tsang Po, the r^2=0.30 and p<0.01; this is a negative correlation, and opposite of what we hypothesized. Therefore, with the exception of the Tsang Po River, where mean annual rainfall is inversely correlated with sinuosity, rainfall and sinuosity are not linearly correlated.

Erosion rates and sinuosity are not linearly correlated for the Mekong and Salween Rivers (r^2 = 0.01, p = 0.75 and r^2 = 0.04, p = 0.46, respectively) (Appendix C). However, for the Yangtze, there is a negative correlation between erosion rate and sinuosity (r^2=0.45 and p=0.02) because it is small number statistics. There are not enough data to do this analysis for the Tsang Po and Irrawaddy Rivers.

Discussion

The main purpose of this study was to investigate multiple potential correlations between sinuosity and the factors thought to affect it. Results from correlation studies show that there are no significant linear correlations between the tested factors and sinuosity for both the entire study area and for most rivers individually. The lack of linear correlations could indicate that the relationship between these factors is non-linear or that other factors may be important in determining sinuosity. These results could also indicate that there may be timescale related problems with our correlations.

Landslides are not linearly correlated with sinuosity. Over the entire area, $r^2=0.00$ and $p>0.05$. This means that almost none of the data are accounted for by a linear trend, and that the data's relationship has a high probability of being random. In addition to this, all of the rivers individually have small r^2 values and p values of greater than 0.05, with the exception of the Tsang Po. The Tsang Po does show a weak positive correlation with landslides, but this is likely due to the fact there are only a few data points, rather than being representative of landslides as a meaningful indicator of sinuosity. This suggests that landslides are not correlated to sinuosity and are likely not a mechanism for increasing sinuosity.

There is similarly no linear correlation between mean annual rainfall, a proxy for climate, and sinuosity. Looking at rainfall in relation to sinuosity for the entire study area, the $r^2=0.00$ and $p>0.05$, meaning that a linear relationship does not fit the data, and that the relationship between variables is random. However in the Tsang Po there is a negative correlation between rainfall and sinuosity $r^2=0.30$ and

$p<0.01$. This is opposite to what I would expect to see, and to what Stark et al. (2010) observed. However, the Tsang Po in this area goes from a broad alluvial river to deeply incised bedrock gorge, which could explain the negative correlation. Taken as a whole, there is not a linear correlation between rainfall and sinuosity. Even though rainfall is not linearly correlated, other proxies for climate such as monsoon strength or storminess may be related.

Erosion rates do not correlate to sinuosity across the study area when taken as a whole. Looking at individual rivers, the Mekong and Salween both have small r^2 values and $p>0.05$, indicating that there is no linear correlation between erosion rates and sinuosity for these two rivers. However, the Yangtze, has a significant negative correlation ($r^2=0.45$ and $p<0.05$). This means that there is a correlation between erosion and sinuosity for the Yangtze, but is likely correlated because there are only 3 different values for erosion rates; furthermore, the correlation is negative, which is the opposite of what we hypothesized. Rainfall and erosion rates have been correlated for the Yangtze, which may indicate a relationship between climate and sinuosity, although that is unlikely because rainfall and sinuosity are not correlated. There is no data available to determine erosion correlations for the Tsang Po and Irrawaddy. Over the entire study area, the results indicate that there is not a linear correlation between basin wide erosion rates and sinuosity.

Due to the fact that there are no overall linear correlations between any of the tested controlling factors and few correlations within river systems induvidually, increases in sinuosity are likely related to other factors. One possible factor to test is a different tectonic proxy. Increasing sinuosity across the area from

east to west mimics patterns in exhumation, a proxy for uplift, across the area. In investigating the role of tectonics, erosion rates were used as a proxy, and no linear correlations were found over the study area between erosion and sinuosity. This could indicate that erosion rates over these rivers are not an accurate proxy for tectonics, and/or that the relationship between erosion rates and tectonics in this area is more complicated than previously considered. While lack of a correlation may rule out tectonics, it is also possible that other parameters could provide more accurate proxies for the tectonic gradient

One possibility is that exhumation rates could serve as a better proxy for tectonics. It has been shown that exhumation across the study area mimics the E-W tectonic gradient (Henck et al. 2011). By looking at where rates of exhumation occur in relation to the rivers, a correlation may show that areas of higher exhumation and therefore increased tectonics could be related to rivers with greater sinuosity.

Other possible factors that could be related to sinuosity in this area are mean local relief and slope. Several studies show correlations between erosion rates and relief (Finnegan et al. 2008; Henck et al. 2011; Larsen and Montgomery 2012; Ouimet et al. 2009). A correlation between these two factors could indicate that the topography controls changes in sinuosity. This relationship could be determined by further GIS analysis by looking at Digital Elevation Models (DEMs) in order to calculate mean local relief and local slope along the rivers.

This study focused on linear relationships between controlling factors, in order to look for initial patterns or correlations. However, non-linear correlations

between parameters may exist. Looking at these parameters for power law or exponential relationships could show correlations.

Conclusion

From looking at correlations between different geomorphic factors and sinuosity, my results show that no correlations exist between the tested parameters, including bedrock, landslides, rainfall and erosion rates. This suggests that on the modern timescales there are no linear relationships between these parameters. While erosion is not correlated with sinuosity across the whole area, it is still possible that tectonics may have a relationship to sinuosity.

These results are interesting because unlike other papers that have found climate, sinuosity and bedrock relationships, such relationships do not exist in the study area. This may indicate that patterns in sinuosity across the eastern Tibetan Plateau are related to other factors. Though erosion is not correlated to sinuosity tectonics could still explain these trends. Moving forward, studying other proxies for tectonics could give insight into how these rivers are changing. For example, looking at mean local relief and slope might also give insight into increasing sinuosity.

Studying the changes in these rivers could indicate information about large-scale landscape changes in an active mountain range. By understanding possible controlling factors that affect sinuosity gives insight into how these parameters affect geomorphological changes and allows for predictions for future changes the evolving landscape.

Acknowledgements

I would like to acknowledge Amanda Schmidt for advising me throughout the duration of this process. I would like to thank Steve Wojtal and Bruce Simonson for being on my committee and providing feedback. I would also like to thank Miriam Rothenberg for reading through multiple drafts, and Lucy Gelb for help with GIS.

References

Akciz, S., Burchfiel, B.C., Crowley, J.L., Yin, J.Y., Chen, L.Z. (2008), Geometry, kinematics, and regional significance of the Chong Shan shear zone, Eastern Himalayan Syntaxis, Yunnan, China, Geosphere, v.4; no. 1, p. 292–314.

Anders, A., Roe, G.H., Montgomery, D.R., Hallet, B., Finnegan, N., and Putkonen, J. (2006), Spatial patterns of precipitation and topography in the Himalya, in Willett, S.D., Hovius, N., Brandon, M.T., and Fisher, D., eds., Tectonics, Climate, and Landscape Evolution: Geological Society of America Special Paper 398, p. 39–53.

Anders, A., Roe, G.H., Montgomery, D.R., and Hallet B. (2008), Influence of precipitation phase on the form of mountain ranges, Geology, v. 36; no. 6, p. 479–482.

Bierman, P.R., and Steig, E.J. (1996), Estimating rates of denudation using cosmogenic isotope abundances in sediment, Earth Surf. Process. Land, v. 21; no. 2, p. 125–139.

Bierman, P., and Montgomery, D.R., 2013 Key Concepts in Geomorphology: Burlington, W.H. Freeman.

Booth, A.L., Page, C., Kidd, W.S.F., and Zeitler, P. (2009), Constraints on the metamorphic evolution of the eastern Himalayan syntaxis from geochronologic and petrologic studies of Namche Barwa, GSA Bulletin, v. 121; no. 3-4, p. 385-407.

Brown, E.T., Stallard, R.F., Larsen, M.C., Raisbeck, G.M., and Yiou, F. (1995), Denudation rates determined from the accumulation of in situ-produced Be-10 in the Luquillo Experimental Forest, Puerto-Rico. Earth Planet. Sci. Lett., v. 129; no. 1–4, p. 193–202.

Burbank, D.W., Blythe, A.E., Putkonen, J., Pratt-Sitaula, B., Gabet, E., Oskin, M., Barros A., and Ojha, T.P., (2003), Decoupling of erosion and precipitation in the Himalayas, Nature, v. 426, p. 652-655.

Burg, J.P., Davy, P., Nievergelt, P., Oberli, F., Seward, D., Diao, Z.Z., and Meier, M. (1997), Exhumation during crustal folding in the Namche-Barwa syntaxis, Terra Nova v. 9; no. 2, p. 53–56.

Clark, M.K., House, M.A., Royden, L.H., Whipple, K.X., Burchfiel, B.C., Zhang, X., Tang, W. (2005), Late Cenozoic uplift of southeastern Tibet. Geology, v. 33; no. 6, p. 525–528

Ding, L., Zhong, D.L., Yin, A., Kapp, P., and Harrison, T.M. (2001), Cenozoic structural and metamorphic evolution of the eastern Himalayan syntaxis (Namche Barwa), Earth Planet. Sci. Lett., v. 192, p.423–438.

Finnegan, N., Hallet, B., Montgomery, D.R., Zeitler, P.K., Stone, J.O., Anders, A.M., and Yuping, L. (2008), Coupling of rock uplift and river incision in the NAamche Barwa-Gyala Peri massif, Tibet, GSA Bulletin, v. 120, p. 142-155.

Gan, W., Zhang, P., Shen, Z.-K, Niu, Z., Wang, M., Wan, Y., Zhou, D., and Cheng, J. (2007), Present-day crustal motion within the Tibetan Plateau indferred from GPS measurements, J. of Geophys. Res., v. 112, B08416.

Granger, D.E., Kirchner, J.W., Finkel, R. (1996), Spatially averaged long-term erosion rates measured from in situ-produced cosmogenic nuclides in alluvial sediment, J. Geol.v. 104; no. 3, p. 249–257.

Hallet, B., and Molnar, P. (2001),, Distorted drainage basins as markers of crustal strain east of the Himalya, J. of Geophys. Res., v. 106 p. 13697-13709.

Harrison, T.M., and Yin, A. (2000), Geologic Evolution of the Himalayan-Tibetan Orogen, Annu. Rev. Earth Planet. Sci. v. 28, p. 211-280.

Hartshorn, K., Hovius, N., Dade, W.B., and Slingerland, R.L. (2012) Climate-Driven Bedrock Incision in an Active Mountain Belt, Science, v. 297; no. 5589, p. 2036-2038.

Henck, A.C., Huntington, K.W., Stone, J.O., Montgomery, D.R., and Hallet, B. (2011), Spatial controls on erosion in the Three Rivers Region, southeastern Tibet and southwestern China, Earth and Planet. Sci. Lett., doi:10.1016/j.espl.2010.12.038.

Hetzel, R. (2013), Active faulting, mountain growth, and erosion at the margins of the Tibetan Plateau constrained by in situ-produced cosmogenic nuclides, Tectonophys., v. 582, p. 1-24.

Hodges, K.V. (2006), A synthesis of the Channel Flow-Extrusion hypothesis as developed for the Himalayan- Tibetan orogenic system, in Channel Flow, Ductile Extrusion, and Exhumation of Lower-Middle Crust in Continental Collision Zones, edited by R. Law, M. Searle and L. Godin, pp.71-90, Geological Society Special Publication, London, 2006.

Larsen, I.J., and Montgomery, D.R. (2012), Landslide erosion coupled to tectonics and river incision, Nature Geoscience, v. 5, p. 468-473.

Map Compilation group, 1986, Geological Map of Nujiang Lancang and Jinsha Rivers Area, scale 1:1000000.

Montgomery, D.R., Balco, G., and Willett, S.D. (2001), Climate, tectonics and the morphology of the Andes, Geology, v. 29; no. 7, p. 579-582.

Montgomery, D.R., and Brandon, M.T. (2002), Topographic controls on erosion rates in tectonically active mountain ranges, Earth and Planet. Sci. Lett., v. 201, p. 481-489.

Mumipour, M., Rezaei-Moghaddam, M.H., and Khorshiddoust, A.M. (2012) Active Tectonics Influence on Drainage Networks in Dinarkooh Region, Zagros Mountain Range, Iran, Geogr. Fis. Din. Quat., v.35, p. 61-68.

Ouimet, W.B., Whipple, K.X., and Granger, D.E. (2009), Beyond threshold hillslopes: Channel adjustment to base-level fall in tectonically active mountain ranges, Geology, v. 37; no. 7, p. 579-582.

Reiners, P.W., Ehlers, T.A., Mitchell, S.G. and Montgomery, D.R. (2003), Coupled spatial variations in precipitation and long-term erosion rates across the Washington Cascades, Nature, v. 426, p. 645-647.

Royden, L.H., Burchfiel, B.C., and van der Hilst, R.D. (2008), The Geological Evolution of the Tibetan Plateau, Science, v. 321, p1054-1058.

Shen, Z.-K., Lu, J., Wang, M., and Bürgmann, R. (2005), Contemporary crustal deformation around the southeast borderland of the Tibetan Plateau, J. of Geophys. Res., v. 110, B11409.

Sklar, D., and Dietrich, W. (2001), Sediment and rock strength controls on river incision into bedrock, Geology, v. 29, p. 1087-1090.

Stark, C.P. (2006), A self-regulating model of bedrock river channel geometry, Geophys. Res. Letters, v. 33, L04402.

Stark, C.P., Barbour, J.R., Hayakawa, Y.S., Hattanji, T., Hovius, N., Chen, H., Lin, C.-W., Horng, M.-J., Xu, K.-Q., and Fukahata, Y. (2010), The Climatic Signature of Incised River Meanders, Science, v. 327, p1497-1501.

Tapponier, P., Zhiqin, X., Roger, F., Meyer, B., Arnaud, N., Wittingler, G., and Jingsui, Y. (2001), Oblique Stepwise Rise and Growth of the Tibet Plateau, Science, v. 294, p. 1671-1677.

Taylor, M., Yin, A., Ryerson, F.J., Kapp, P., and Ding, L. (2003), Conjugate strike-slip faulting along the Bangong-Nujiang suture zone accommodates coeval east-west extension and north-south shortening in the interior of the Tibetan Plateau, Tectonics, v. 22; no. 4, 1044.

Taylor, M., and Yin, A. (2009), Active structures of the Himalayan-Tibetan orogeny and their relationships to earthquake distribution, contemporary strain field, and Cenozoic volcanism, Geosphere, v. 9; no 3, p199-214.

Yang, T.-N., Hou, Z.-Q., Wang, Y., Zhang, H.-R., and Wand, Z.-L. (2012), Late Paleozoic to Early Mesozoic tectonic evolution of northeast Tibet: Evidence from the Triassic composite western Jinsha-Garze-Litang suture, Tectonics, v. 34, TC4004.

Zhang, P.-Z., Shang, Z., Wang, M., Gan, W., Bürgmann, R., Molnar, P., Wang, Q., Niu, Z., Sun, J., Wu, J., Hanrong, S., and Xinzhao, Y. (2004), Continuous deformation of the Tibetan Plateau from global positioning system data, Geology, v. 32; no. 9, p. 809-812.

Appendix A: Landslides

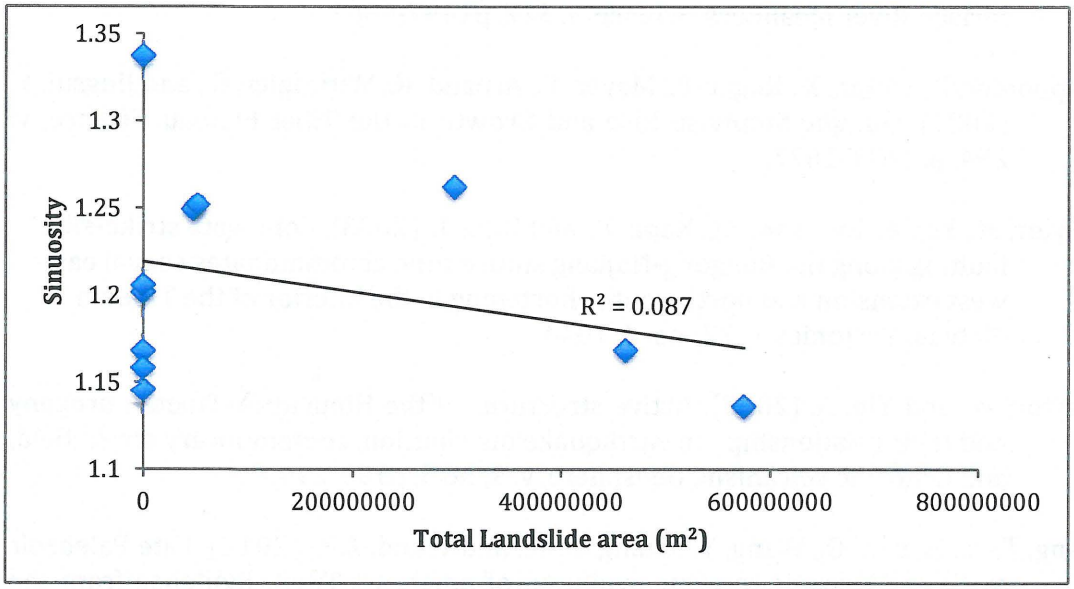

Appendix A1: Graph of linear correlation between total landslide area and sinuosity for the Yangtze. No linear correlation exists, and r^2=0.09 and p=0.36.

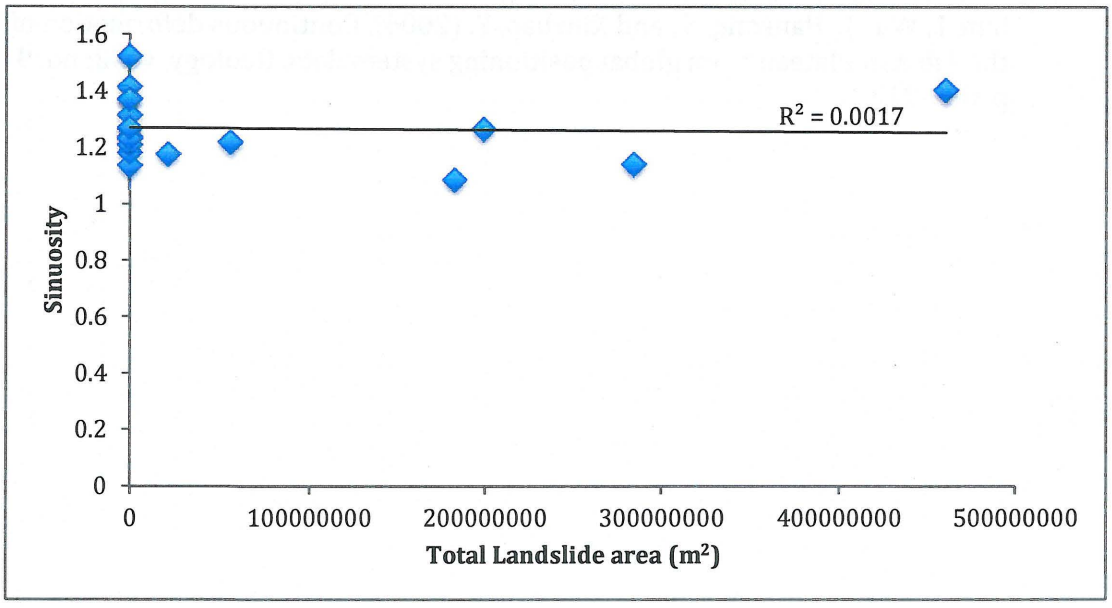

Appendix A2: Graph of linear correlation between total landslide area and sinuosity for the Mekong. No linear correlation exists, and r^2=0.00 and p=0.87.

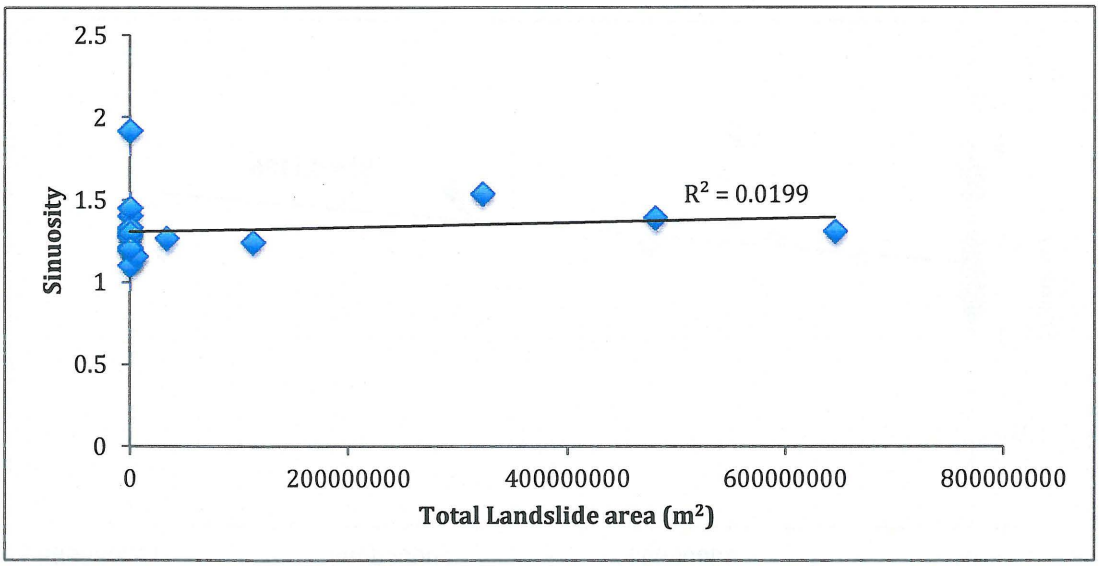

Appendix A3: Graph of linear correlation between total landslide area and sinuosity for the Salween. No linear correlation exists, and r^2=0.02 and p=0.56.

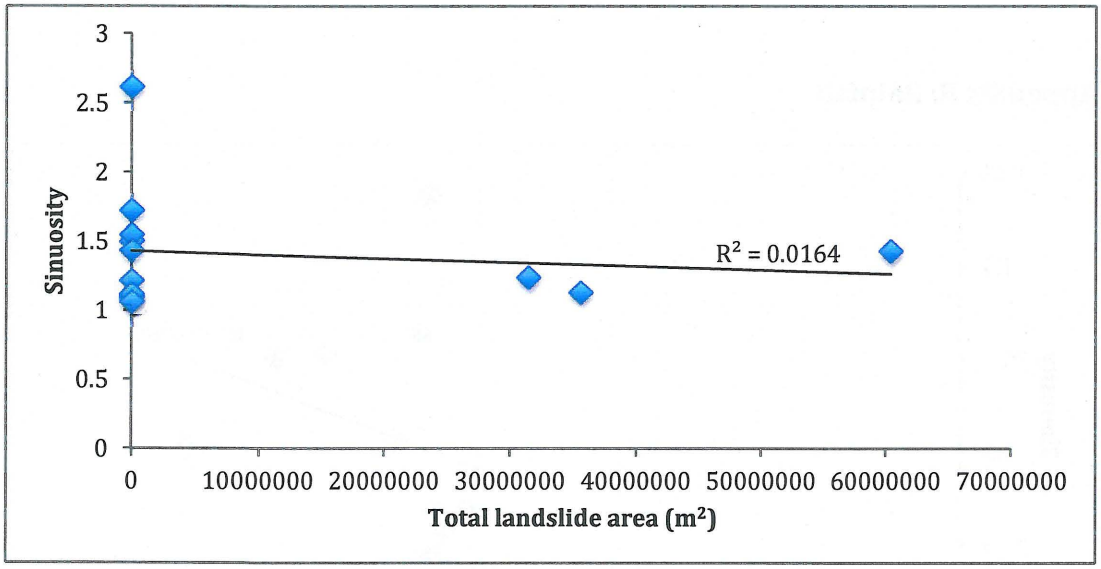

Appendix A4: Graph of linear correlation between total landslide area and sinuosity for the Irrawaddy. No linear correlation exists, and r^2=0.02 and p=0.67.

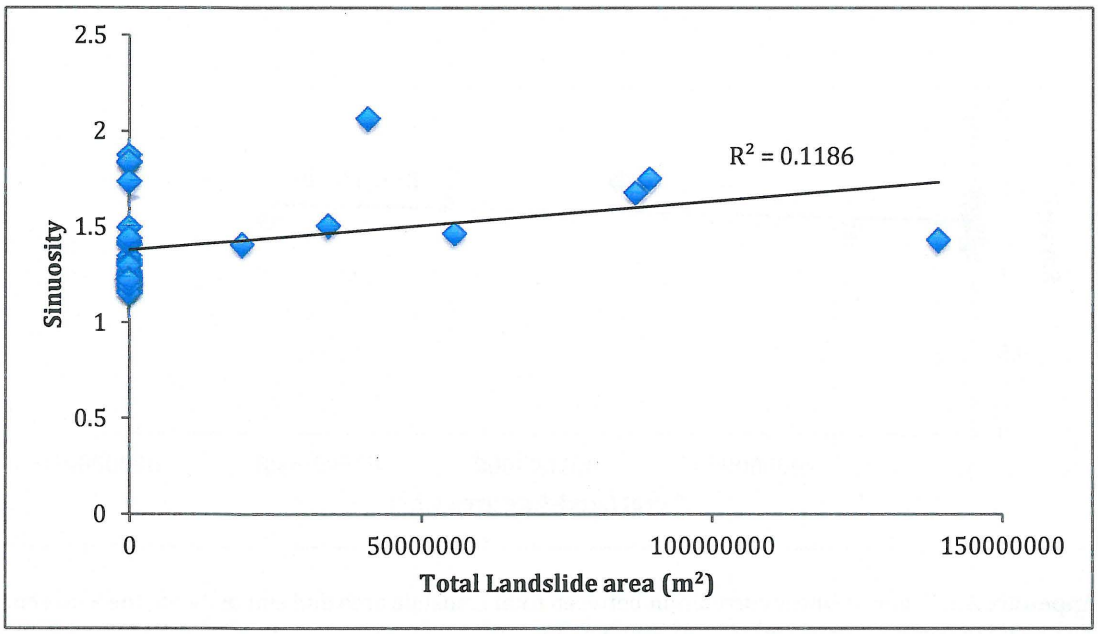

Appendix A5: Graph of linear correlation between total landslide area and sinuosity for the Tsang Po. No linear correlation exists, and r^2=0.12 and p=0.05.

Appendix B: Rainfall

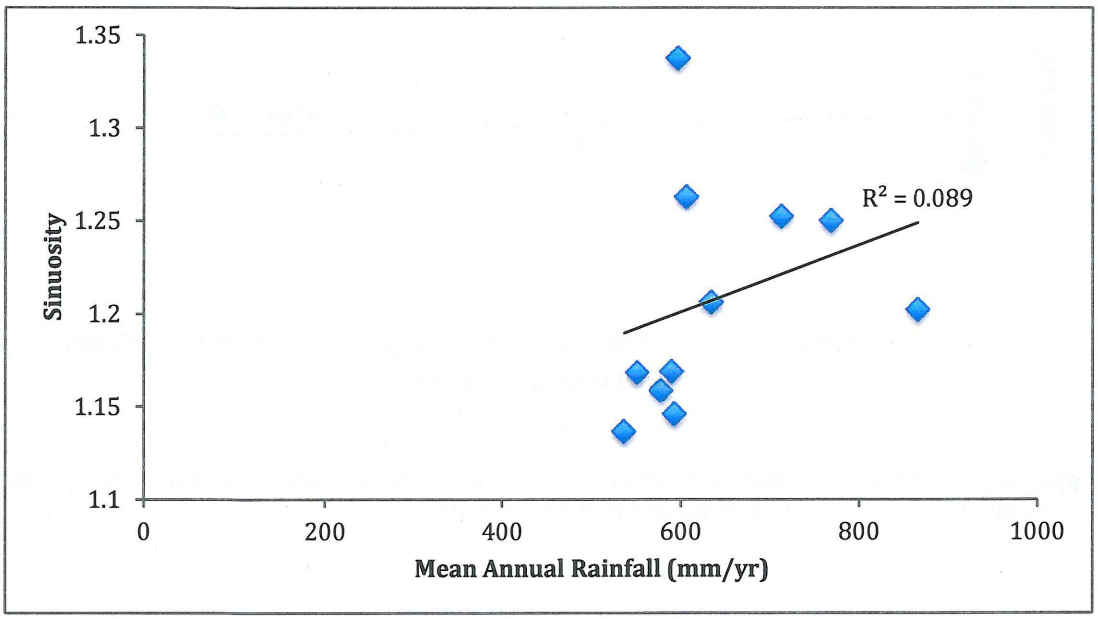

Appendix B1: Graph of linear correlation between mean annual rainfall and sinuosity for the Yangtze. No linear correlation exists, and r^2=0.09 and p=0.37.

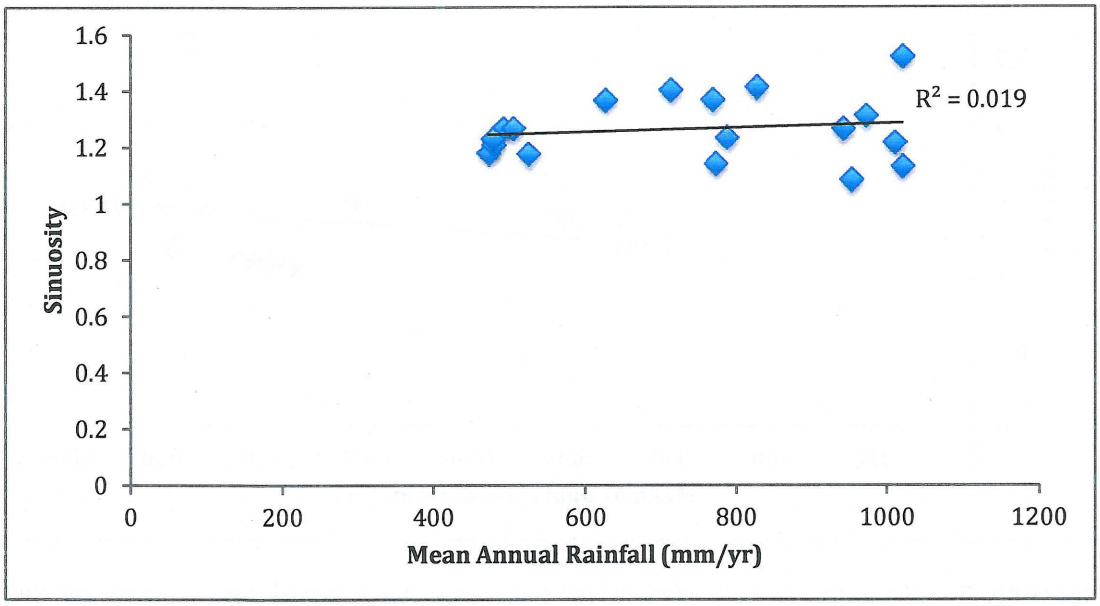

Appendix B2: Graph of linear correlation between mean annual rainfall and sinuosity for the Mekong. No linear correlation exists, and r^2=0.02 and p=0.58.

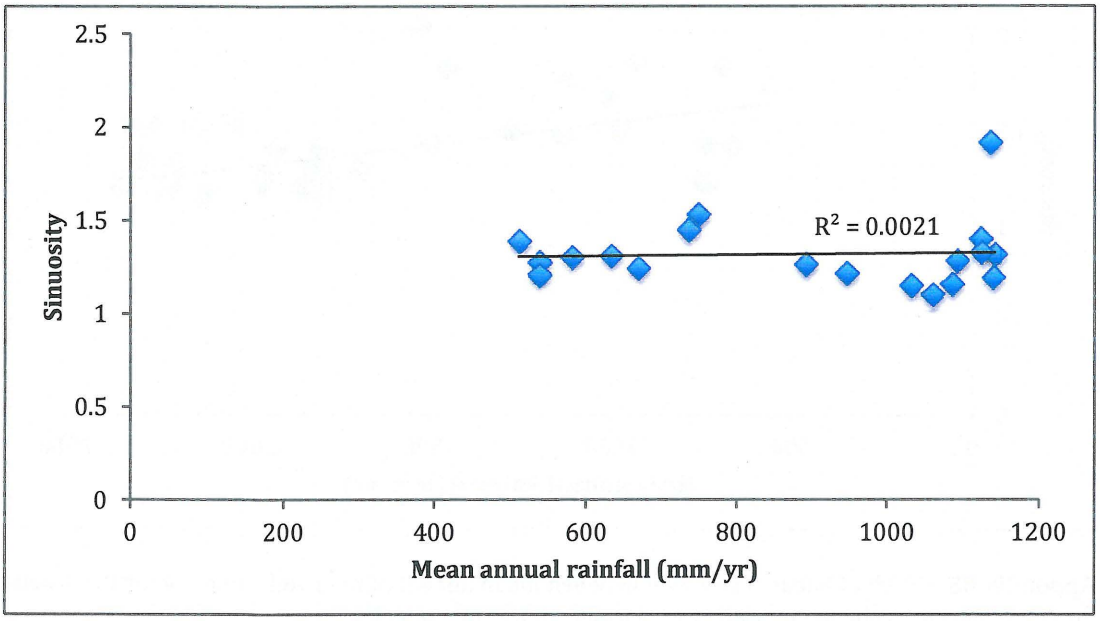

Appendix B3: Graph of linear correlation between mean annual rainfall and sinuosity for the Salween. No linear correlation exists, and r^2=0.00 and p=0.85.

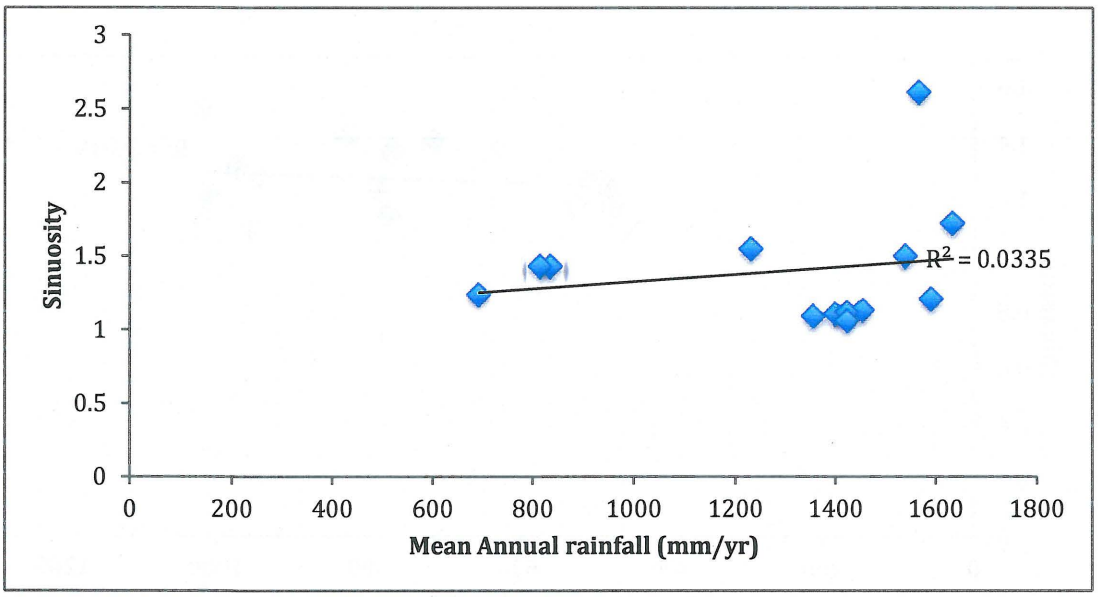

Appendix B4: Graph of linear correlation between mean annual rainfall and sinuosity for the Irrawaddy. No linear correlation exists, and $r^2=0.03$ and $p=0.82$.

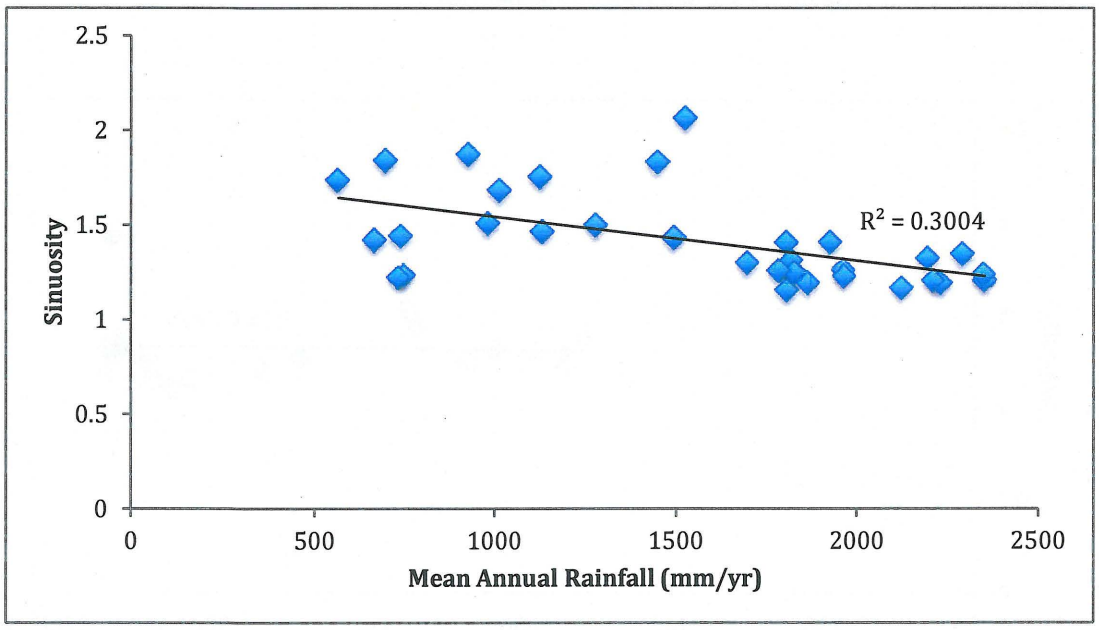

Appendix B5: Graph of linear correlation between mean annual rainfall and sinuosity for the Tsang Po. A weak negative linear correlation exists, and $r^2=0.30$ and $p<0.01$.

Appendix C: Erosion Rates

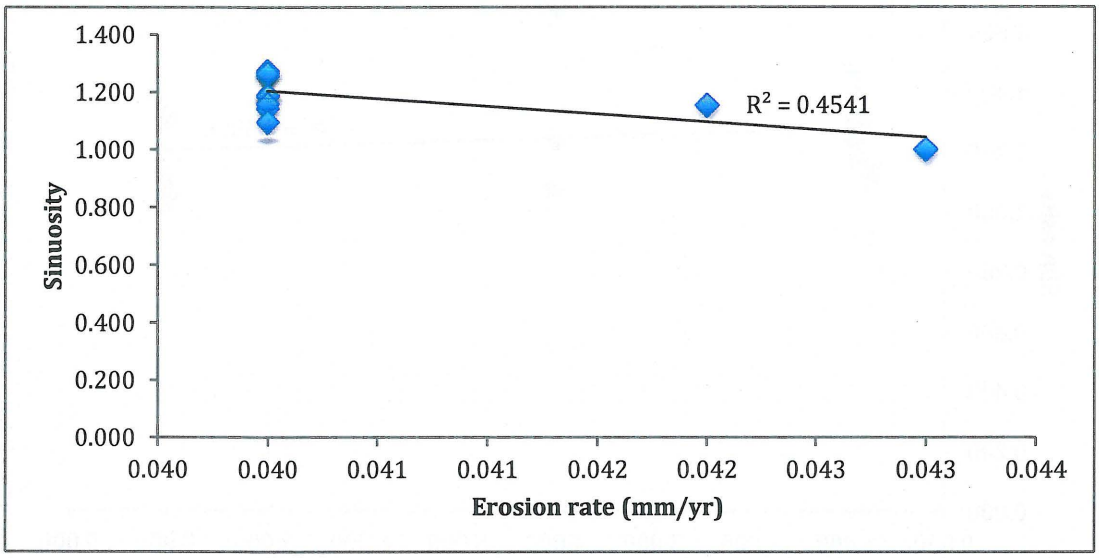

Appendix C1: Graph of linear correlation between erosion rate and sinuosity for the Yangtze. A weak linear correlation exists, and r^2=0.45 and p=0.02.

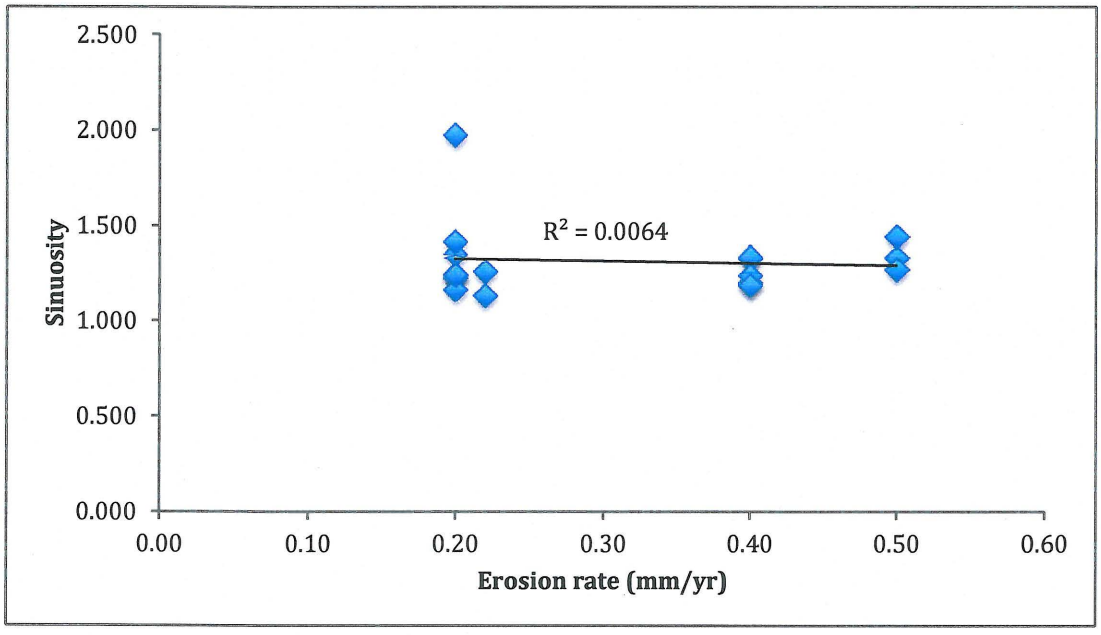

Appendix C2: Graph of linear correlation between erosion rate and sinuosity for the Mekong. No linear correlation exists, and r^2=0.01 and p=0.75.

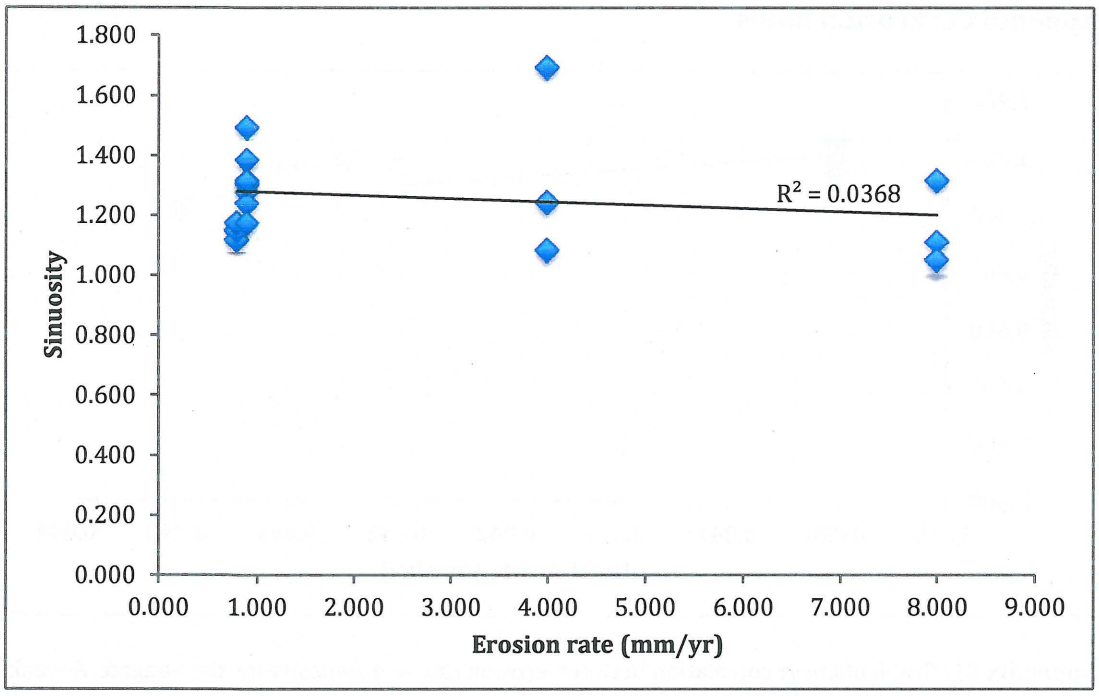

Appendix C3: Graph of linear correlation between erosion rate and sinuosity for the Salween. No linear correlation exists, and r^2=0.04 and p=0.46.